genes

MDPI

Article

A Head-to-Head Comparison of AAV9 Biodistribution in Mice: Routes of Administration and Age Dependence

Matthew Rioux †, Andrea Boitnott †, Satvik Paduri, Yuhui Hu and Steven J. Gray *

Department of Pediatrics, UT Southwestern Medical Center, Dallas, TX 75390, USA
* Correspondence: steven.gray@utsouthwestern.edu
† These authors contributed equally to this work.

Abstract

Background/Objectives: Adeno-associated virus serotype 9 (AAV9) can cross the blood–brain barrier, making it widely used as a gene delivery vector for central nervous system (CNS) applications. Despite extensive use of AAV9 in translational research, variability in study designs makes cross-comparisons difficult to interpret. We designed a study in mice to generate a resource of AAV9 biodistribution across tissues for commonly used routes of administration and treatment ages. Methods: Lumbar intrathecal, intracerebroventricular, lumbar intrathecal and intracerebroventricular combination, or intravenous injections of vehicle or AAV9/GFP were performed in C57BL/6J male and female mice on postnatal day 1, 5, 10, or 28. Organs were collected at postnatal day 56 and biodistribution of AAV9/GFP was evaluated by quantifying GFP protein expression and vector genome copy number. Results: Direct cerebrospinal fluid injections led to higher transgene expression levels in the brain and spinal cord compared to intravenous administration but did not de-target transgene expression in peripheral tissues. Lumbar intrathecal and intracerebroventricular combination injections resulted in expression throughout the CNS but did not substantially increase expression in either the spinal cord or brain beyond the levels obtained with the respective single routes. Treatment age had effects on AAV9 biodistribution regardless of the route of administration, especially in the brain, eye, and liver. Conclusions: Our results provide the necessary biodistribution data to establish a standardized benchmark for comparison of the current gold standard AAV9 to next generation viral vectors. Additionally, this body of work can provide valuable insights for the design of translational gene therapy studies.

Keywords: gene therapy; AAV9; biodistribution; route of administration; treatment age; central nervous system; peripheral tissues

Check for updates

Academic Editor: Jiri Forejt

Received: 10 November 2025
Revised: 6 January 2026
Accepted: 29 January 2026
Published: 9 February 2026

Copyright: © 2026 by the authors. Licensee MDPI, Basel, Switzerland. This article is an open access article distributed under the terms and conditions of the Creative Commons Attribution (CC BY) license.

1. Introduction

Adeno-associated virus serotype 9 (AAV9) is a widely adopted gene therapy vector for targeting neurons and central nervous system (CNS) tissue due to its ability to cross the blood–brain barrier [1–5]. Since its discovery [6], several groups have published on AAV9 biodistribution across species and various factors that can alter AAV9 transduction in different cell and tissue types. Some of these factors include preexisting immunity to AAV [7–9], genome design (single-stranded vs. self-complementary) [5,10], capsid engineering [11], regulatory elements [11,12], physical body positioning [13], and critical to this paper, route of administration [14–16], and treatment age [2,17].

Route of administration is typically chosen based on the study's application—the characteristics of a disease or gene of interest—but there are also practical considerations like ease of use in a clinical setting and the total dose required to achieve efficacy while maintaining safety. A systemic intravenous (IV) route of administration is used in multiple FDA approved in vivo AAV-mediated gene therapies and is simple to perform in a clinical setting [18–22]. However, there are limitations with IV administration of AAV9, especially for targeting the brain, where efficiency is low [11,23]. Specific for CNS-directed targeting, an alternative to IV administration is direct cerebrospinal fluid (CSF) administration by an intracerebroventricular (ICV), lumbar intrathecal (IT), or intracisternal magna (ICM) injection. Compared to IV administration, direct CSF injections allow for lower doses to achieve widespread CNS transduction, but transduction in peripheral tissue is maintained to a substantial extent [16,24,25]. One example is AAV9 gene therapy for spinal muscular atrophy, where a recently approved product, Itvisma® (Novartis Gene Therapies), uses lumbar IT administration with lower total vector dose than Zolgensma® (Novartis Gene Therapies), the IV approved product, thereby reducing systemic exposure while maintaining effective CNS transduction [20,26].

Among the various direct CSF routes of administration, some biodistribution effects appear consistent across studies; however, direct comparisons are limited by differences in study design. Few studies have directly compared ICV and lumbar IT administration of AAV9, but available data suggest a general brain-wide advantage for ICV, with notable areas of the CNS that are transduced higher or lower by each route [27,28]. Peripheral tissue is also transduced well, especially muscle and heart, with these direct CSF administration routes. Studies have looked at how ICM administration affects AAV9 biodistribution and showed some advantages for brain transduction with this route compared to IT administration, especially in the hindbrain near the cisterna magna [29,30]; however, since a prior direct comparison between IT and ICM routes was previously published by our lab, this comparison was excluded from the present study and will not be discussed further in this paper.

Combination routes of administration have potential to increase transduction in relevant brain regions even further; but, only a handful of studies have been published on dual administration routes and benefits have not been clearly shown in AAV-mediated applications [31,32]. A combination IV and ICV route of administration of AAV9 was used in an expanded access trial for one patient with Canavan disease [33]. The results suggest that the increased vector distribution resulting from the dual administration route may improve treatment outcomes.

In addition to route of administration, treatment age has been focused on as a factor that can influence AAV9 biodistribution. For direct CSF injections, the consensus is that transduction in the brain is better at younger ages [17]. In the eye, treatment age highly influences transduction, where specific time windows in early postnatal development seem to be optimal [34,35]. Treatment age also highly influences transduction in the liver, where older animals show higher transduction than younger animals [34].

In this study, we compared the biodistribution of AAV9 from IT, ICV, or IT & ICV combination injections to a systemic IV injection. Each of these injection routes were performed at timepoints across early postnatal development, at postnatal day 1, 5, 10, or 28. The goal was to create a resource for AAV9 distribution in CNS tissue and peripheral organs to guide gene therapy study designs and to establish standardized expression data for comparisons with novel capsids. Our results corroborate many previous studies, showing that direct CSF administration is superior at transducing the CNS compared to systemic IV administration but has minimal effects on peripheral tissue targeting. In general, ICV administration provided better overall brain transduction while IT administration

provided better spinal cord transduction, although both resulted in substantial transduction of both targets. The combined IT & ICV route resulted in expression in both the brain and spinal cord but did not substantially increase expression in either region beyond the levels obtained with the respective single routes. Consistent with most prior investigations, earlier treatment age resulted in higher transduction efficiency in the brain, whereas peripheral organ transduction was not overly influenced, with exceptions in the eye and liver.

2. Materials and Methods

2.1. Mice

All procedures were approved by UT Southwestern Medical Center's Institutional Animal Care and Use Committee (protocol number: 2018-102422). Female and male C57BL/6J mice (strain #000664, The Jackson Laboratory) were bred to generate all mice in this study. The mice were housed in a controlled facility on a 12 h light/dark cycle and provided with food and water ad libitum. 16% protein-irradiated chow was used, except for in breeding cages, which received 18% protein-irradiated chow.

2.2. Viral Vector

A previously published self-complementary adeno-associated virus serotype 9 vector highly expressing enhanced green fluorescent protein (AAV9/CBh-EGFP-BGHpA) was used for this study [36]. The viral vector was manufactured by the UNC Viral Vector Core by triple transfection of suspension HEK293 cells, as previously described [37]. The vector was formulated in PBS containing 5% D-sorbitol with a total NaCl concentration of 350 mM, and this formulation buffer was used as the vehicle and diluent in all experiments. Viral vector titer was measured with the Stunner instrument (Unchained Labs). Long term storage of the viral vector was maintained at −80 °C and thawed aliquots were stored at 4 °C.

2.3. Study Design

Even numbers of female and male mice were injected at postnatal day 1, 5, 10, or 28 with either vehicle, AAV9/GFP at a low dose of 2.5×10^{11} vg, or AAV9/GFP at a high dose of 5×10^{11} vg. Doses were not adjusted to age or body weight; however, body and organ weights were taken from a separate cohort of mice at each timepoint to estimate how vector load may scale with growth (Figure A1, Table A1). Injections were either CNS directed into the CSF—lumbar IT, ICV, or a combination of both—or systemic via IV administration. The volume injected varied by treatment age and route of administration (Table 1). Mice were monitored regularly for overall health, and body weights were taken once a week.

2.4. Lumbar Intrathecal (IT) Injection

The lumbar IT injection was performed as previously described [38].

2.5. Intracerebroventricular (ICV) Injection

Pups at postnatal day 1 or 5 were cryoanesthetized until fully sedated and moved to a pre-cooled clay mold to stabilize the body for a freehand bilateral ICV injection. A stereotaxic injection syringe (65460-06, Hamilton, Reno, NV, USA) with a 33 GA needle (65461-02, Hamilton) set to a stop depth of 2 mm was used and needle placement was determined based on lambda, the midline, and the eye, such that if a line was drawn from lambda to the eye, the placement would be 1 mm from lambda towards the eye and about 0.5 mm from midline. A light was used to help visualize the skull suture lines under the skin. A total of 1.3 µL was injected over 1 min per hemisphere, with a subsequent 30 s hold before withdrawing the needle. This is a modified protocol from what has been previously

described [39]. Pups were paw-tattooed for identification and placed on a heating pad until fully conscious before returning to their home cage.

Table 1. Injection volumes and number of mice enrolled for each treatment group.

Treatment Age	Route of Administration	Dose (vg)	Total Volume (µL)	AAV9 (n)	Vehicle (n)
P1	IV	2.5×10^{11}	20	10	2
	ICV	2.5×10^{11}	2.6	10	2
	IT	2.5×10^{11}	2.6	8	2
	IT & ICV	2.5×10^{11}	4	8	2
P5	IV	2.5×10^{11}	20	10	2
		5×10^{11}	20	10	2
	ICV	2.5×10^{11}	2.6	10	2
	IT	2.5×10^{11}	5.1	10	0
		5×10^{11}	5.1	3 [1]	3
	IT & ICV	2.5×10^{11}	6.3	10	2
		5×10^{11}	6.3	6	4
P10	IT	2.5×10^{11}	5.1	9	2
		5×10^{11}	5.1	11	2
P28	IV	5×10^{11}	50	11	2
	ICV	2.5×10^{11}	2.6	10	2
	IT	5×10^{11}	5.1	10	2
	IT & ICV	5×10^{11}	6.2	10	2

[1] Not fully enrolled due to a high mortality rate.

Mice at postnatal day 28 were anesthetized with an isoflurane and oxygen mixture (3% induction and 1–1.5% maintenance) and placed on a stereotaxic apparatus for bilateral ICV injection. Body temperature was maintained throughout the procedure with a heat pad. A small incision was made in the skin over the skull. The lateral ventricles were targeted using the Allan Brain Atlas coordinates AP −0.3, ML +/−1.0, DV −3.0 and a 5 µL Hamilton syringe with a 33G needle was used to deliver the injection solution at rate of 0.5 µL/min (Micro4 MicroSyringe Pump Controller, World Precision Instruments, Sarasota, FL, USA). The skin was closed with sutures (Size 5-0 PDS II Suture, Ethicon, Somerville, NJ, USA). A 2% sterile lidocaine solution was used as a local anesthetic, and 0.05 mg/kg buprenorphine and 5 mg/kg carprofen were used as post-op analgesics.

2.6. Lumbar Intrathecal (IT) & Intracerebroventricular (ICV) Combination Injection

A dual route of administration combining the lumbar IT injection and the ICV injection was performed using the protocols described above. The total vector dose was evenly split between the two routes. To allow for complete CSF turnover [40], the ICV injection was performed 4 h after the lumbar IT injection.

2.7. Intravenous (IV) Injection

Pups at postnatal day 1 or 5 were injected intravenously via the superficial temporal vein. The pups were restrained and 20 µL was injected slowly using a 30G insulin syringe, with a subsequent 15 s hold before withdrawing the needle. Pressure was applied to the injection site until bleeding ceased. This is a modified protocol from what has been

previously described [39]. Pups were paw-tattooed for identification and returned to their home cage.

Mice at postnatal day 28 were injected intravenously via the lateral tail vein using a tube restraint (Mouse Tail Illuminator, Braintree Scientific, Braintree, MA, USA) and standard techniques. The tail was warmed by radiant heat from the device light for 1 min. The tail was then swabbed with a 70% isopropyl alcohol pad and rotated ¼ turn. An insulin syringe with a 30G needle was inserted into the vein. Following visualization of blood into the syringe, 50 µL was injected slowly. The needle was withdrawn, and pressure was applied to the injection site until bleeding ceased. The mice were removed from the restraint and returned to the home cage.

2.8. Tissue Harvest

Necropsies were performed on postnatal day 56. Mice were anesthetized with 2,2,2-tribromoethanol (421430500, Thermo Scientific Chemicals, Haverhill, MA, USA) dissolved in 2-methyl-2-butanol (152463, Sigma-Aldrich, St. Louis, MI, USA) and diluted in sterile water to a final concentration of 2.5%, prepared fresh on the day of use. A dose of 500 mg/kg was administered intraperitoneally to achieve rapid, non-recovery anesthesia. Following full anesthesia, the chest cavity was opened and blood was collected by cardiac puncture using a 1 mL syringe fitted with a 25G needle. The mice were then perfused with PBS and tissue was collected for downstream processing. Tissue from the mouse's right side was flash frozen on dry ice and tissue from the mouse's left side was fixed in 10% formalin for 24 h before being transferred to 70% ethanol and then processed for paraffin embedding. The cornea of eyes collected for fixation were punctured with a 30G needle before fixation and after standard fixation; the eyes were then transferred to 50% ethanol for 24 h and finally to 70% ethanol until paraffin embedding. Tissues collected included: cerebrum, cerebellum, cervical spinal cord, thoracic spinal cord, lumbar spinal cord, sciatic nerve, heart, lung, liver, kidney, spleen, gonad, triceps, small intestine, large intestine, tongue, and eye. For the separate cohort of mice used to determine growth rates, necropsies (as described above) were performed on postnatal day 1, 5, 10, 28, or 56. Following the perfusion with PBS, each organ was removed in its entirety, gently patted dry, and weighed on a precision balance (ME303E, Mettler Toledo, Columbus, OH, USA).

2.9. Histology

Paraffin processing of fixed tissues was performed according to standard procedures [41,42]. In brief, cassetted organs in 70% ethanol were dehydrated through six increasing grades of ethanol, cleared through three exchanges of xylene, and infiltrated with three exchanges of paraffin (39602004, Leica, Germany) with vacuum assist using a Excelsior Tissue Processor (Thermo Scientific). Processing times on the automated tissue processor ranged from 6 to 28 h based on tissue size and lipid content. Samples were oriented in metal molds for final embedding in paraffin using a paraffin embedding station (Leica EG1150H) and cut into 5 µm sections on a microtome (Leica RM2235) before staining.

For hematoxylin and eosin (H&E) staining, slides were deparaffinized with xylene and rehydrated with an ethanol gradient, then washed in running tap water for 5 min, followed by incubation in Richard-Allan Hematoxylin for 4 min. The slides were then washed in distilled water twice for 10 min each, followed by being dipped in Eosin solution for 1 min, dehydrated with an ethanol gradient, and cleared with xylene before being mounted with mounting medium.

Immunohistochemistry (IHC) was performed on a group mean-representative subset of mice from the biodistribution qPCR analysis. These two to three mice were selected because their GFP vector DNA values were around the mean across all tissues. The ImmPRESS

excel amplified horseradish peroxidase polymer staining kit (MP-7601, Vector Laboratories, USA) was used for GFP IHC staining. All steps were performed at room temperature unless noted. Slides were deparaffinated by xylene and rehydrated with gradually reduced ethanol. Antigen retrieval was performed with Antigen Unmasking Solution (H-3300, Vector Laboratories). Slides were then incubated with BLOXALL Blocking solution (SP-6000, Vector Laboratories) for 10 min. Slides were washed with 1X PBS for 5 min, then incubated with 2.5% normal horse serum for 30 min. Slides were then incubated with rabbit Anti-GFP antibody (Abcam, UK, ab183735), diluted 1:1000 in normal horse serum, at 4 °C overnight. Then slides were washed with distilled water and 1X PBS and incubated with Amplifier Antibody (goat anti-rabbit, IgG) for 20 min. Slides were washed with PBS and incubated with ImmPRESS Polymer Reagent for 30 min and washed with distilled water and 1X PBS. Finally, slides were incubated with ImmPACT DAB EqV working solution until desired stain intensity developed. Then slides were washed with distilled water and counterstained with Modified Mayer's hematoxylin.

Following staining, a NanoZoomer S60 (Hamamatsu Photonics, Japan) was used for whole slide imaging and HALO (Indica Labs, USA) was used for quantitative image analysis.

2.10. DNA Extraction

Whole tissue samples were disrupted and homogenized using 5 mm metal beads and a TissueLyser II (Qiagen, The Netherlands). The entire piece of tissue frozen at necropsy was used, except for the kidney, in which only the top third was used. Lysis buffer ATL (Qiagen) was pre-warmed to 37 °C before use and the volume varied by tissue type: cerebrum —700 µL; cerebellum and triceps—300 µL; cervical spinal cord, lumbar spinal cord, and sciatic nerve—180 µL; liver—1100 µL; and heart, lung, and kidney—500 µL. Proteinase K was also added at a 1:9 ratio with buffer ATL. The cerebrum, cerebellum, liver, heart, triceps, lungs, and kidney were shaken at 30 Hz for 2.5 min before the block was rotated 180° and shaken again at 30 Hz for 2.5 min to ensure even lysis. The cervical spinal cord, lumbar spinal cord, and sciatic nerve were shaken at 15 Hz for 1.5 min before being rotated and shaken again at 15 Hz for 1.5 min. The kidney and liver samples were then incubated in a thermomixer at 56 °C, shaking at 1000 rpm for 3 h. The rest of the tissues were incubated in a thermomixer at 56 °C, shaking at 1000 rpm for 1 h. After incubation, the samples were centrifuged with a mini centrifuge to separate any debris. In total, 200 µL of each sample was loaded on a 96-well S Block for DNA extraction using the QIAamp DNA kit and a QIAcube HT instrument (Qiagen). The preloaded QIAamp DNA Extraction protocol was used. The DNA samples were eluted in AE buffer (Qiagen) and stored at −30 °C.

2.11. Quantitative PCR (qPCR)

qPCR was performed on a LightCycler 480 (Roche Diagnostics, Switzerland) using SYBR Green (04887352001, Roche Diagnostics) to determine the amount of double-stranded copies of GFP DNA present in the purified DNA samples. GFP (Forward primer: AGCAGCACGACTTCTTCAAGTCC; Reverse primer: TGTAGTTGTACTCCAGCTTGTGCC, Sigma-Aldrich) was normalized to mouse GAPDH (Forward primer: CATCACTGCCACCCAGAAGACTG; Reverse primer: ATGCCAGTGAGCTTCCCGTTCAG, Sigma-Aldrich). During downstream analysis, samples where GAPDH diploid copies/µL were <50 or not detected were removed from analysis. Samples where GFP vg/diploid genome was not detected, but GAPDH diploid copies/µL were >50, were removed from analysis for AAV9/GFP injected mice; however, for vehicle injected mice, the not detected values were changed to 0.

2.12. Statistics

Data were analyzed blind to treatment group. Statistics and plots were generated using custom R scripts. For the survival curves, a log-rank test was used to compare treatment groups. For the quantitative PCR analysis, pairwise Wilcoxon rank-sum tests were used to compare GFP vg/diploid genome between two treatment groups, followed by Benjamini–Hochberg control of False Discovery Rate correction to the p-values within a tissue and treatment age subset. The adjusted p-value is depicted on the plots as significant stars where * $0.01 < p \leq 0.05$, ** $0.001 < p \leq 0.01$, *** $0.0001 < p \leq 0.001$, and **** $p \leq 0.0001$. Statistics were not performed on GFP immunohistochemistry-calculated, percent-DAB-area-stained plots due to low numbers.

3. Results

3.1. Localized High Expression of GFP Can Cause Adverse Effects in Mice

At early developmental treatment timepoints and with certain routes of administration, significant adverse effects and mortality were observed in response to AAV9/GFP (Figure 1, Table A2). These adverse effects presented in mostly hind quarter, neurologic abnormalities including ataxia, paralysis of one or both hind limbs, tremors, and overall poor body condition. These mice were euthanized according to veterinary direction and included as death events in the survival analysis along with mice that died naturally. A significant difference in survival among P1 injection treatment groups was observed (Figure 1a). AAV9/GFP injected via the IT route caused a 47% mortality rate with an average age at termination of 10 days. The IT & ICV route caused a 39% mortality rate with an average age at termination of 18 days. No deaths were recorded from ICV or IV administration of AAV9/GFP, nor were any deaths recorded from a vehicle injection administered by either of the four administration routes. Additionally, a significant difference in survival among P5 injection treatment groups was observed (Figure 1b). IT administration of AAV9/GFP at 5×10^{11} vg caused a 70% mortality rate and at 2.5×10^{11} vg caused a 17% mortality rate, both with an average age at termination of 19 days. IT & ICV administration of AAV9/GFP at 5×10^{11} vg caused a 40% mortality rate with an average age at termination of 19 days. However, at 2.5×10^{11} vg no deaths were recorded. ICV administration of AAV9/GFP at 2.5×10^{11} vg caused a 17% mortality rate with an average age at termination of 21 days. No deaths were recorded from IV administration of AAV9/GFP at either dose. There was one mouse that died after an ICV injection of vehicle; however, no other deaths were recorded from a vehicle injection administered by the other routes of administration. No significant differences in survival among P10 or P28 injection treatment groups were observed. Additionally, no significant differences in weight were observed for any group.

To explore the cause of death, H&E staining was performed on tissues taken at necropsy from euthanized mice. The most significant findings were in the spinal cord (Figure 1c–f, Table A2). Nerve fiber degeneration, characterized by vacuolation of the white matter tracts, were common findings and affected variably sized areas of the tissue. All terminated mice reviewed displayed some degree of abnormality in the spinal cord, but notably no abnormality in the dorsal root ganglion. A representative example of focal area degeneration in the cervical spinal cord is provided (Figure 1d), with a normal cervical spinal cord section for comparison (Figure 1c). In some mice, the spinal cords contained scattered degenerating neurons and endothelial cell hypertrophy. A representative lumbar spinal cord section including these abnormalities, in addition to a diffuse area of degeneration, is provided (Figure 1f), with a normal lumbar spinal cord section for comparison (Figure 1e).

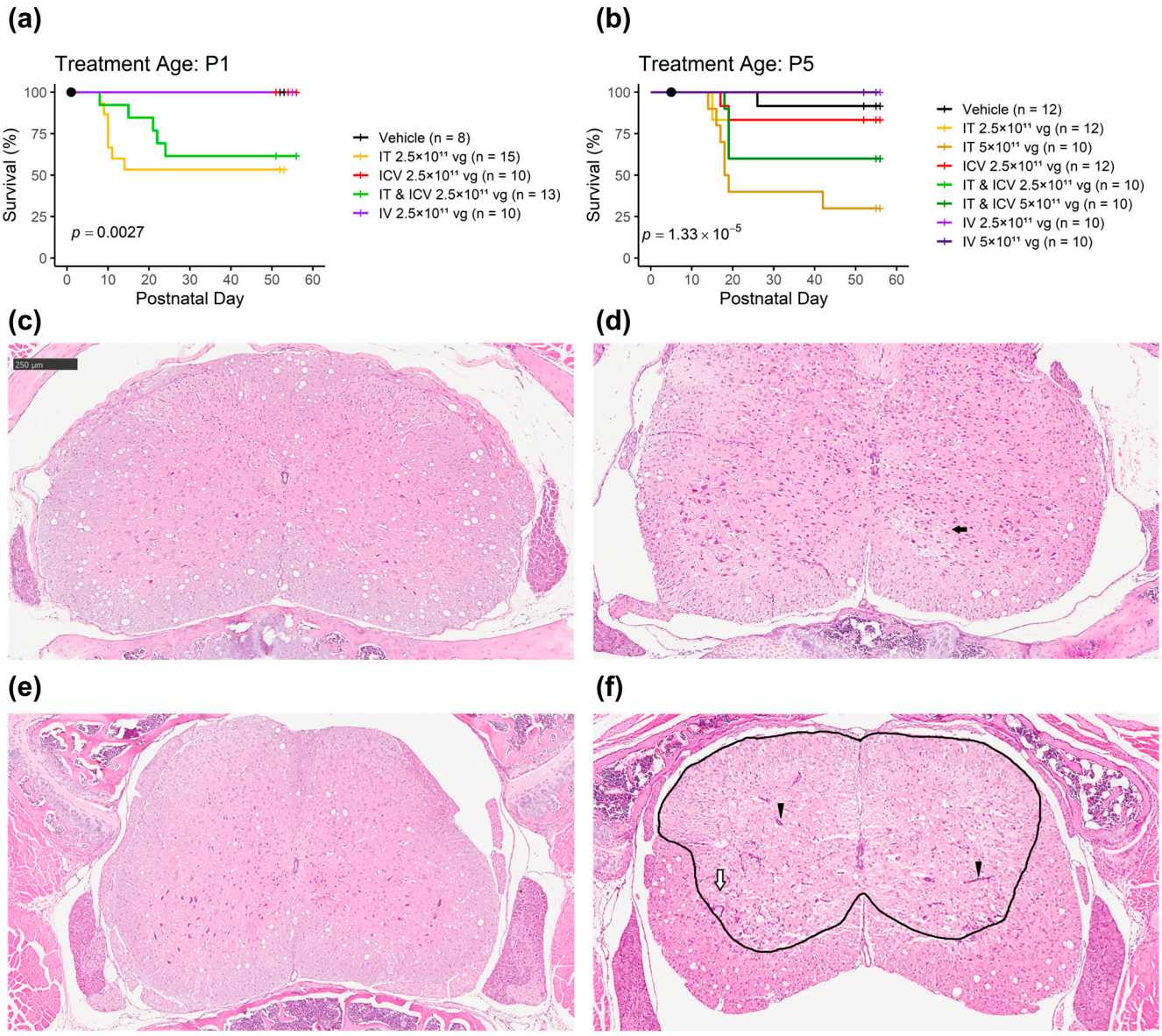

Figure 1. Survival curves of mice in each treatment group after injection at (**a**) P1 or (**b**) P5. Black dot indicates the time point of injection. H&E staining of a representative (**c**) normal cervical spinal cord, (**d**) cervical spinal cord with a focal area of degeneration (black arrow), (**e**) normal lumbar spinal cord, and (**f**) lumbar spinal cord with a diffuse area of degeneration (circled in black), endothelial hypertrophy (black arrows), and degenerating neurons (white arrow). All sections are at 5× magnification, 250 µm scale bar.

Summary: High localized expression of GFP can cause nerve fiber degeneration and toxicity in mice. Because IT and IT & ICV injections deliver the vector in immediate proximity to the spinal cord, they are expected to produce higher local transduction in this tissue compared to ICV or IV injection. The adverse effects are therefore unlikely due to route of administration or treatment age alone. Younger mice, at P1 and P5 treatment, received a higher vector dose per body weight compared to older mice because the doses were fixed and not adjusted for weight or tissue size. Additionally, at both P1 and P5, IT administration alone resulted in more mortality than IT & ICV administration, which aligns with the hypothesis that high local expression in the spinal cord is the main driver of toxicity, because the IT & ICV injection splits the dose between the two routes so the IT portion is half the IT alone injection. Furthermore, the adverse effects were dose-dependent, with

higher doses leading to increased lethality, further supporting a GFP localized expression mechanism rather than an effect of route of administration or treatment age.

3.2. Direct Cerebrospinal Fluid Injection of AAV9/GFP Increases Transduction in the Mouse Brain Compared to IV Administration

IT, ICV, or IT & ICV routes of administration that target the CNS by delivery into the CSF induce higher transgene expression across the brain compared to systemic IV administration (Figure 2). For P1 injections of AAV9/GFP at 2.5×10^{11} vg, ICV and IT & ICV administration increased biodistribution, and IT administration trended towards increased biodistribution of the caudal brain compared to IV administration (Figure 2a). All direct CSF routes of administration also showed increased biodistribution in the rostral brain compared to IV administration. For P5 injections, AAV9/GFP was dosed at 2.5×10^{11} or 5×10^{11} vg and no significant changes in biodistribution were observed from changing the dose within each route of administration (Figure A11). For comparisons within the same dose group, direct CSF routes of administration increased biodistribution in both the caudal and rostral brain compared to IV administration, except for IT administration of AAV9/GFP at 2.5×10^{11} vg, which showed a trending increase in rostral brain transduction but was not significant. Additionally, for comparisons within the same dose group, IT & ICV administration increased biodistribution to the caudal brain compared to either IT or ICV administration alone. The increase in biodistribution from the combination route was also seen as a trend in the rostral brain. Additionally, AAV9/GFP biodistribution after ICV administration was increased compared to IT administration in the caudal and rostral brain. For P28 injections of AAV9/GFP, ICV and IT & ICV administration increased biodistribution in the caudal brain compared to IV administration and compared to IT administration. Biodistribution to the rostral brain showed less of an effect from route of administration; however, ICV administration did increase biodistribution compared to IV administration, and the other direct CSF routes trended in the same way. To note, the ICV injection of AAV9/GFP at P28 was dosed at 2.5×10^{11} vg, whereas for the other routes of administration AAV9/GFP was dosed at 5×10^{11} vg.

The biodistribution findings in the brain were corroborated by GFP IHC (Figures 2b,c, A2–A5, A11, vehicle comparison in Figure A10a). While sample numbers were insufficient for statistical analysis, quantification of GFP-positive area showed a similar route of administration trends within each treatment age (Figure 2b). The GFP IHC whole brain images (Figure 2c) further illustrate how expression patterns change with route of administration and treatment age by revealing differences in specific brain regions, including the cortex, hippocampus, midbrain, subcortex, thalamus/hypothalamus, cerebellum, and pons/medulla (Figures A2–A5).

Summary: IT, ICV, and IT & ICV routes of administration are superior at transducing the brain compared to IV administration at all time points of intervention. While an IT & ICV combination injection significantly increased transduction in the brain compared to IT administration at all time points, IT & ICV combination injection did not substantially increase transduction in the brain compared to ICV administration, except for in the caudal brain at P5. Additionally, regardless of route of administration, GFP expression in younger mice appeared to be higher than in older mice.

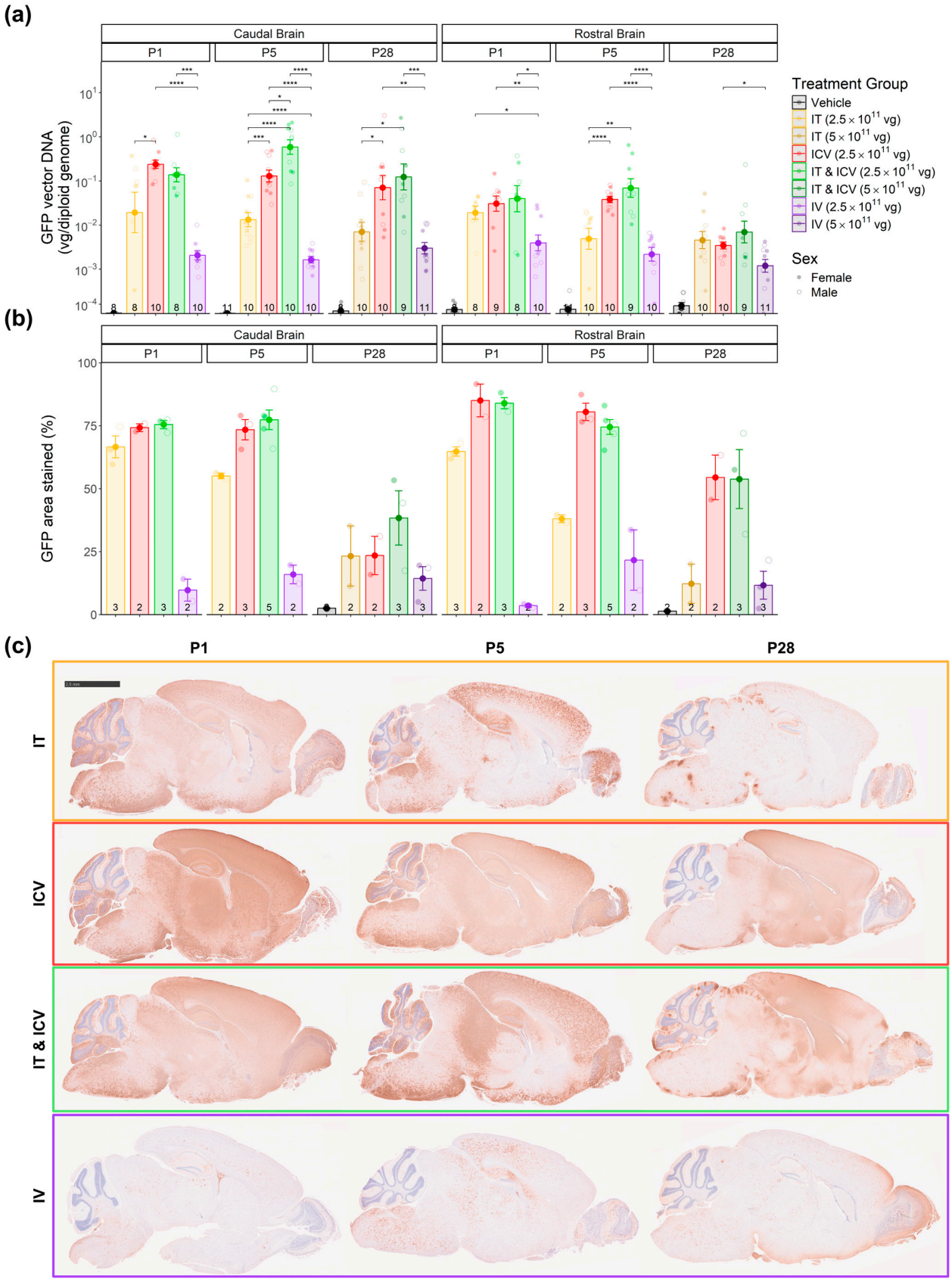

Figure 2. Expression of AAV9/GFP in the brain. (**a**) GFP vector DNA as measured by qPCR in the caudal and rostral brain for each treatment group after injection at P1, P5, or P28. Mean and standard error of the mean values are included in Table A3. (**b**) GFP expression as measured by percent DAB area stained in the caudal and rostral brain for each treatment group after injection at P1, P5, and P28.

The subset of samples for IHC analysis represent mice around the mean GFP vector DNA values across all tissues. (**c**) Representative images of brain sections stained for GFP by IHC. Images are from the 2.5×10^{11} vg dose, except for P28 IT, IT & ICV, and IV, which are from the 5×10^{11} vg dose. All sections are at 1.5× magnification, 2.5 mm scale bar. * $0.01 < p \leq 0.05$, ** $0.001 < p \leq 0.01$, *** $0.0001 < p \leq 0.001$, **** $p \leq 0.0001$. Error bars indicate standard error of the mean.

3.3. Direct Cerebrospinal Fluid Injection of AAV9/GFP Increases Transduction in the Mouse Spinal Cord Compared to IV Administration

Like in the brain, IT, ICV, or IT & ICV routes of administration that target the CNS by delivery into the CSF induce higher transgene expression in the spinal cord compared to systemic IV administration (Figure 3). For P1 injections of AAV9/GFP at 2.5×10^{11} vg, ICV and IT & ICV administration increased biodistribution, and IT administration trended towards increased biodistribution of the cervical and lumbar spinal cord compared to IV administration (Figure 3a). However, no differences were observed when comparing across the direct CSF routes in the cervical or lumbar spinal cord. For P5 injections, AAV9/GFP was dosed at 2.5×10^{11} or 5×10^{11} vg, and no significant changes in biodistribution were observed from changing the dose within each route of administration, except for lumbar spinal cord transduction from IV administration, which did show increased biodistribution with increased dose (Figure A11). For comparisons within the same dose group, all direct CSF routes of administration increased biodistribution to both the cervical and lumbar spinal cord compared to IV administration. Additionally, ICV administration either trended toward lower AAV9/GFP biodistribution or was significantly lower compared to IT or IT & ICV administration. For P28 injections of AAV9/GFP, all direct CSF routes of administration showed increased biodistribution in the cervical spinal cord compared to IV administration, but this effect was not observed in the lumbar spinal cord. Like at P5, ICV administration caused a decrease in biodistribution to both the cervical and lumbar spinal cord compared to the other CNS targeting routes of administration; however, in the cervical spinal cord the comparison to IT administration was only a trend and not significant. As noted previously, at P28 the ICV injection of AAV9/GFP was dosed at 2.5×10^{11} vg, whereas for the other routes of administration AAV9/GFP was dosed at 5×10^{11} vg.

The biodistribution findings in the spinal cord were corroborated by GFP IHC (Figure 3b,c, vehicle comparison in Figure A10b). While sample numbers were insufficient for statistical analysis, quantification of GFP-positive area showed a similar route of administration trends within each treatment age (Figure 3b). GFP IHC spinal cord images further illustrate how expression patterns change with route of administration and treatment age (Figure 3c). An added advantage of the spinal cord GFP IHC was the ability to assess expression in the whole spine, including in the dorsal root ganglion. Expression in the dorsal root ganglion has been associated with toxicity in AAV-mediated gene therapy studies, but it has been shown that mice may be less prone to this specific toxicity than rats or non-human primates [43–46]. GFP IHC suggests that all routes of administration and treatment ages result in transgene expression in the cervical and lumbar dorsal root ganglion (Figure A6); however, it remains unclear if route of administration or treatment age effects the amount of transgene expression in this region.

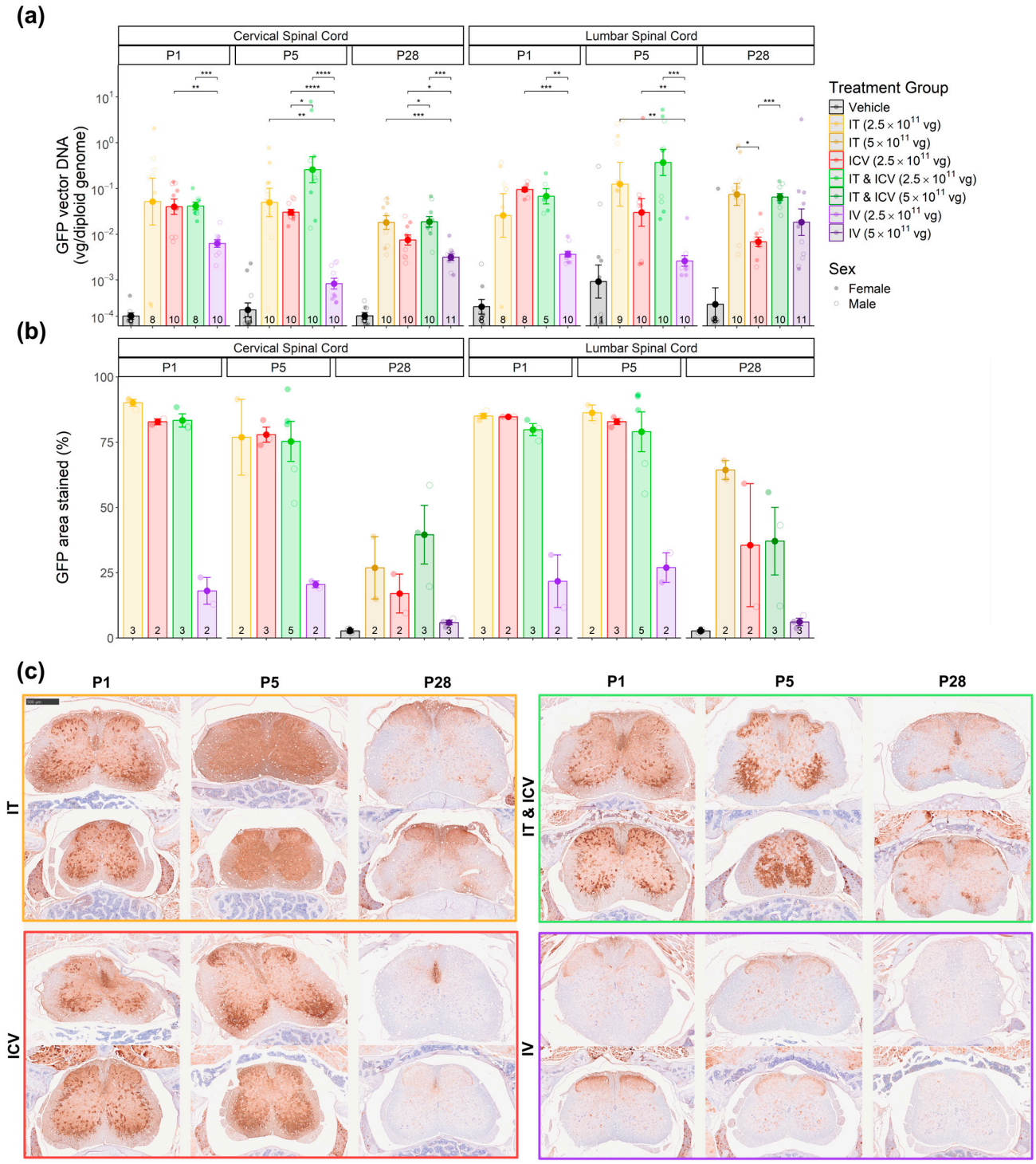

Figure 3. Expression of AAV9/GFP in the spinal cord. (**a**) GFP vector DNA as measured by qPCR in the cervical and lumbar spinal cord for each treatment group after injection at P1, P5, or P28. Mean and standard error of the mean values are included in Table A3. (**b**) GFP expression as measured by percent DAB area stained in the cervical and lumbar spinal cord for each treatment group after injection at P1, P5, or P28. The subset of samples for IHC analysis represent mice around the mean GFP vector DNA values across all tissues. (**c**) Representative images of cervical spinal cord (**top**) and lumbar spinal cord (**bottom**) sections stained for GFP by IHC. Images are from the 2.5×10^{11} vg dose, except P28 IT, IT & ICV, and IV, which are from the 5×10^{11} vg dose. All sections are at 5× magnification, 500 µm scale bar. * $0.01 < p \leq 0.05$, ** $0.001 < p \leq 0.01$, *** $0.0001 < p \leq 0.001$, **** $p \leq 0.0001$. Error bars indicate standard error of the mean.

Summary: IT, ICV, and IT & ICV routes of administration are superior at transducing the spinal cord compared to IV administration at most time points of intervention. At some time points, IT & ICV combination injection significantly increased transduction in the spinal cord compared to ICV administration, but not IT administration. The DRG is transduced by all routes of administration and at all treatment ages Additionally, regardless of route of administration, GFP expression in younger mice appeared to be higher than in older mice.

3.4. Direct Cerebrospinal Fluid Injection of AAV9/GFP Results in Substantial Peripheral Tissue Biodistribution Comparable to IV Administration

Direct CSF routes of administration would be expected to target peripheral organs to a lesser extent compared to IV administration. However, our data showed comparable vector biodistribution and transgene expression in peripheral tissues across all routes of administration (Figures 4, 5 and A7–A9). Muscle transduction was assessed in the heart, triceps, and tongue (Figure 4). Route of administration did not clearly affect AAV9/GFP biodistribution in the heart or triceps, except that in the heart at treatment age P5, IT & ICV administration showed increased biodistribution compared to IT or IV administration, and in the triceps at treatment age P28, both IT and IV administration showed increased biodistribution compared to ICV and IT & ICV administration (Figure 4a). Like the heart and triceps, the tongue had a high expression of GFP (Figure 4b), suggesting that muscle is highly targeted from all routes of administration with this vector.

Liver transduction was most affected by age rather than route of administration, where P28-treated animals showed the highest GFP expression levels (Figure 5a). Age effects on liver transduction have been previously described with the thought that high regeneration rates in the liver of young mice dilute out transgene expression over time [34]. However, modest route of administration differences were observed for P1 injections, where IV administration increased transduction compared to IT and IT & ICV administration. Additionally, for P28 injections, IT & ICV administration increased transduction compared to IT or ICV injections alone, and IV administration increased transduction compared to ICV administration.

Route of administration affected transduction in the kidney the most out of all peripheral tissues assessed (Figure 5a). For P1 injections, IT & ICV administration increased AAV9/GFP biodistribution compared to IT or IV administration. For P5 injections, AAV9/GFP was dosed at 2.5×10^{11} or 5×10^{11} vg, and no significant changes in biodistribution were observed from changing the dose for IT or IV administration, but for IT & ICV administration, increased biodistribution was observed with increased dose (Figure A11). For AAV9/GFP at 2.5×10^{11} vg comparisons, IT, ICV, and IV administration all showed increased biodistribution compared to IT & ICV administration (Figure 5a), but this was not observed at 5×10^{11} vg (Figure A11). For P28 injections, IT, IT & ICV, and IV administration all increased biodistribution compared to ICV administration.

In lung tissue, ICV administration at P5 resulted in decreased biodistribution compared to IT and IV administration of AAV9/GFP at 2.5×10^{11} vg, and this pattern was also seen at treatment age P28, where ICV administration resulted in decreased biodistribution compared to all other routes of administration (Figure 5a).

The biodistribution findings in peripheral tissue were corroborated by GFP IHC histological examination and quantification (Figures 4b,c and 5b,c, vehicle comparison in Figure A10c). IHC was performed on additional peripheral tissue, including spleen, small intestine, large intestine, testes, and ovaries for each route of administration (Figures A7–A9, vehicle comparison in Figure A10c). Notably, no transgene expression was observed in germ cells within the gonads.

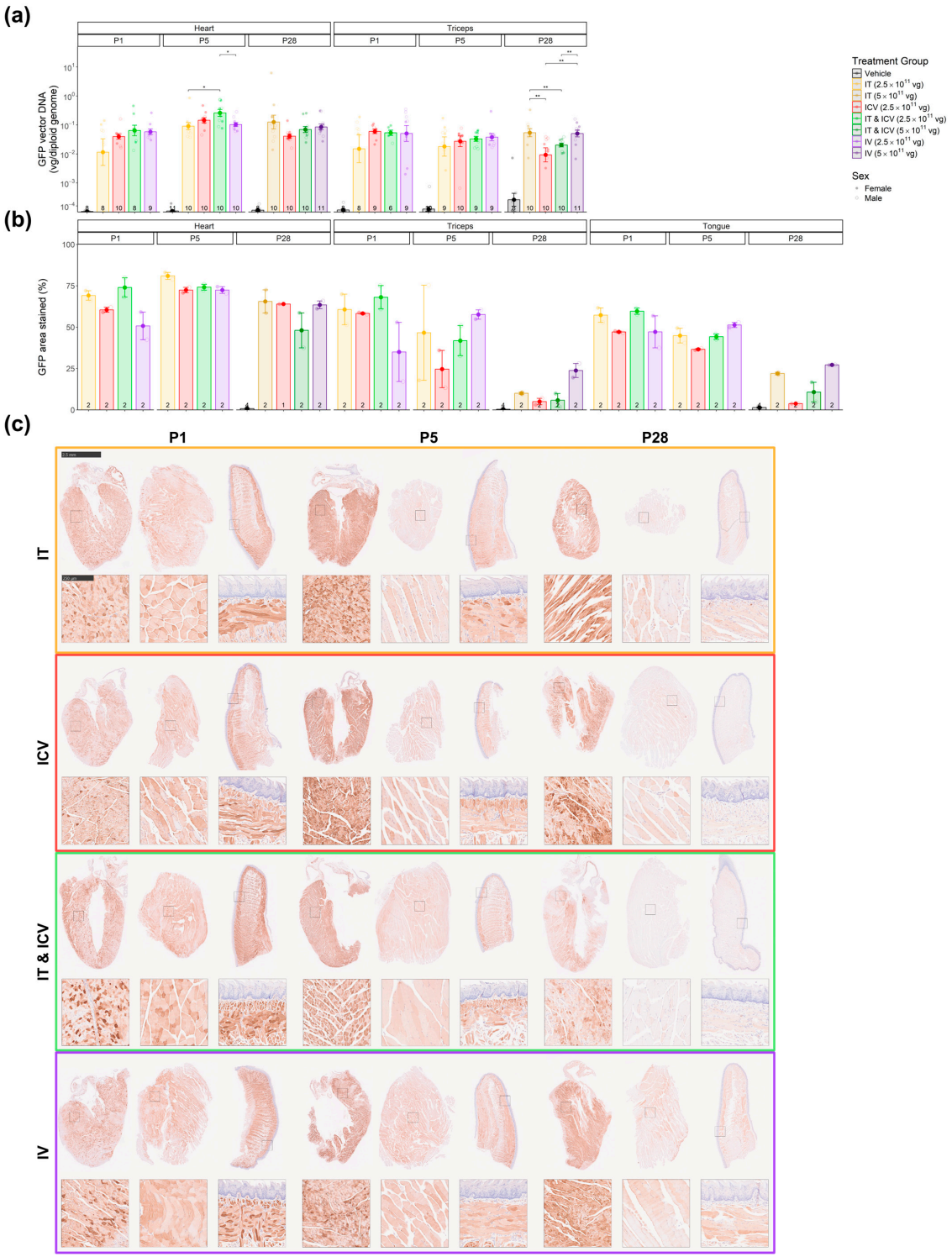

Figure 4. Expression of AAV9/GFP in the muscle. (**a**) GFP vector DNA as measured by qPCR in the heart and triceps for each treatment group after injection at P1, P5, or P28. Mean and standard error of the mean values are included in Table A3. (**b**) GFP expression as measured by percent DAB area stained in the heart, triceps, and tongue for each treatment group after injection at P1, P5, or P28. The subset of samples for IHC analysis represent mice around the mean GFP vector DNA values across all tissues. (**c**) Representative images of heart (**left**), triceps (**middle**), and tongue (**right**) sections stained for GFP by IHC. Images from the 2.5×10^{11} vg dose are shown except P28 IT, IT & ICV, and IV (5×10^{11} vg dose). Full organ sections (**top**) are at 1.25× magnification, 2.5 mm scale bar. Black squares show inset location. The magnified insets (**bottom**) are at 10× magnification, 250 µm scale bar. * $0.01 < p \leq 0.05$, ** $0.001 < p \leq 0.01$. Error bars indicate standard error of the mean.

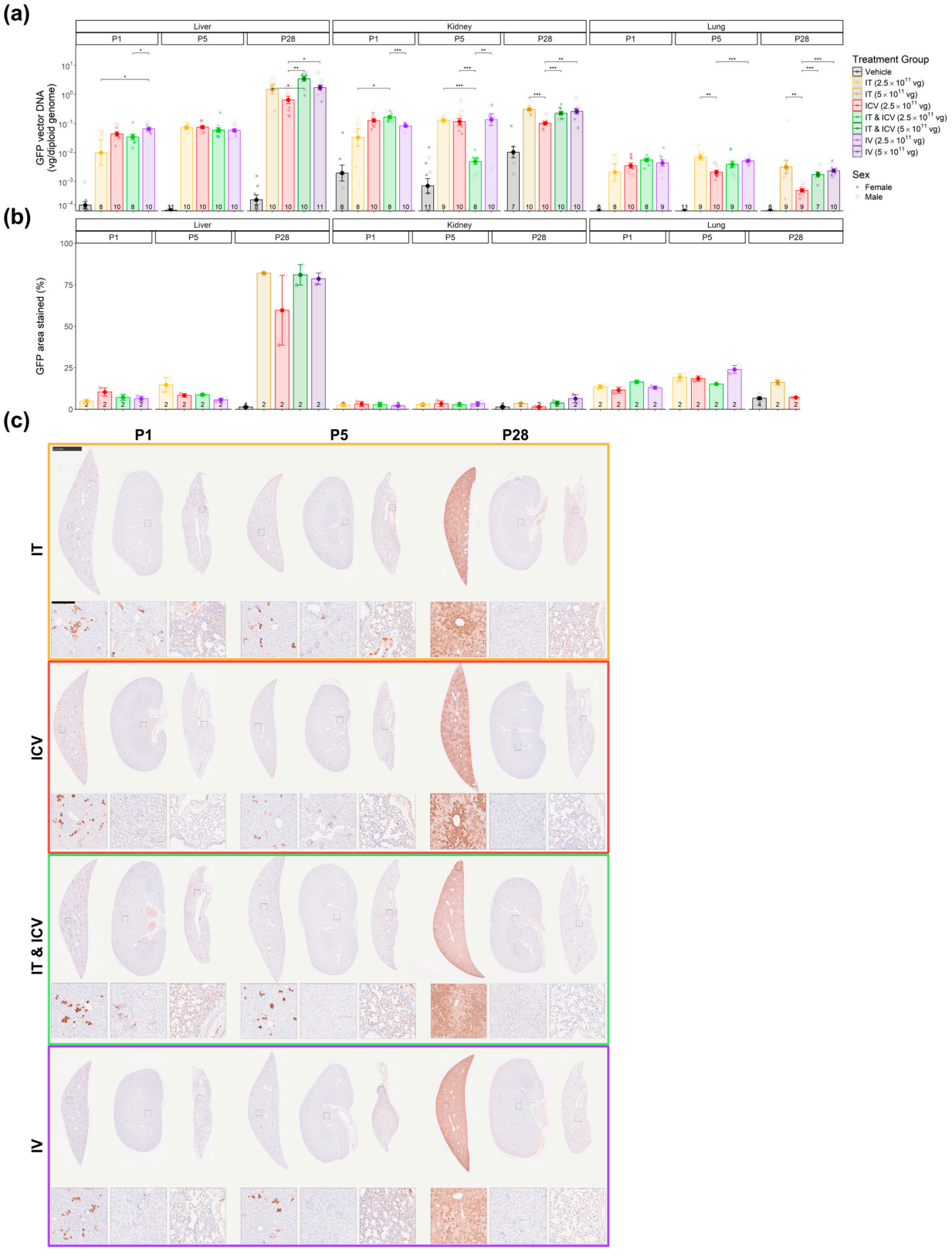

Figure 5. Expression of AAV9/GFP in other peripheral tissues. (**a**) GFP vector DNA as measured by qPCR in the liver, kidney, and lung for each treatment group after injection at P1, P5, or P28. Mean and standard error of the mean values are included in Table A3. (**b**) GFP expression as measured by percent DAB area stained in the liver, kidney, and lung for each treatment group after injection at P1, P5, or P28. The subset of samples for IHC analysis represent mice around the mean GFP vector DNA values across all tissues. (**c**) Representative images of liver (**left**), kidney (**middle**), and lung (**right**)

sections stained for GFP by IHC. Images from the 2.5 × 10^{11} vg dose are shown except P28 IT, IT & ICV, and IV (5 × 10^{11} vg dose). Full organ sections (**top**) are at 1.25× magnification, 2.5 mm scale bar. Black squares show inset location. The magnified insets (**bottom**) are at 10× magnification, 250 µm scale bar. * $0.01 < p \leq 0.05$, ** $0.001 < p \leq 0.01$, *** $0.0001 < p \leq 0.001$. Error bars indicate standard error of the mean.

Summary: IT, ICV, and IT & ICV routes of administration transduce peripheral tissue to a similar extent as IV administration. Expression in muscle tissue is high compared to expression in other peripheral tissue regardless of route of administration or treatment age, except at P28, where GFP expression is reduced in the triceps and tongue compared to earlier treatment ages. The opposite effect occurs in the liver, where higher transduction is observed with treatment at older ages, regardless of route of administration.

3.5. The Eye Is Transduced by All Routes of Administration, with the Amount of Transduction Being Mostly Affected by Age

All routes of administration transduced the eye to some extent (Figure 6). The amount of transduction was scored on a low = 1, medium = 2, or high = 3 scale. Representative histological images for each score are provided for visualization along with a vehicle control (Figure 6b–e). For P1 injections, IT, IT & ICV, and IV administration resulted in a transduction score of about 2, whereas ICV administration scored 1 (Figure 6a). For P5 injections, all routes and doses scored between 2 and 3. For P10 injections, IT administration resulted in a transduction score of about 2. All injections at P28 scored around 1 regardless of route of administration.

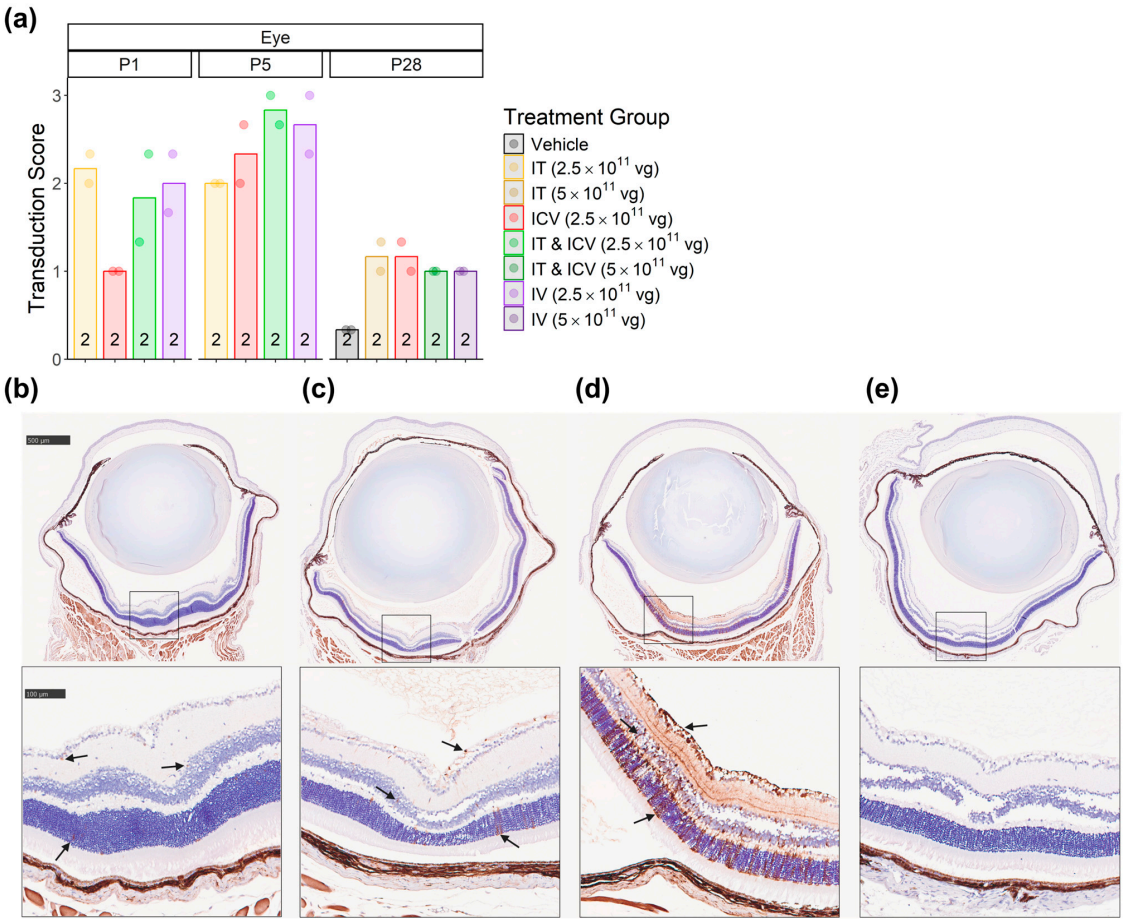

Figure 6. Expression of AAV9/GFP in the eye. (**a**) GFP transduction in the retina, qualitatively measured as amount of DAB area stained by IHC for each treatment group after injection at P1, P5, or P28. Transduction score 1 = low transduction, 2 = mid transduction, 3 = high transduction.

Representative images of eye sections that (**b**) score a 1, (**c**) score a 2, (**d**) score a 3 are shown next to (**e**) a vehicle control. Black arrows (**b–d**) show examples of positive GFP staining in different layers of the retina. Whole eye sections (**top**) are at 5× magnification, 500 µm scale bar. Black squares show inset location. Magnified insets (**bottom**) at 20× magnification, 100 µm scale bar.

Summary: P5 is an optimal age for ocular transduction regardless of route of administration. This aligns with a previous AAV9/GFP IV administration study, which showed treatment at P5 results in higher retina expression than treatment at P1, P3, P7, and P9 [35]. That publication also provides a more detailed characterization of the transduced cell types. Additionally, our P1 results showing reduced tranduction from ICV administration compared to IV administration aligns with another previous study which tested an AAV9 gene replacement therapy in a mouse model of Sanfilippo syndrome and found most benefit in the retina with neonatal IV administration compared to ICV administration [47].

4. Discussion

When interpreting the data in this study, it is important to understand that the dose is total vector genomes and is not calculated to normalize for mouse size. To directly compare all routes of administration, a fixed dose was used rather than a dose per unit of body weight. Doses 2.5×10^{11} and 5×10^{11} vg were chosen for translational relevance to doses used in humans, where a 2.5×10^{11} vg mouse dose approximates to a 1.00×10^{15} vg human dose [16]. No significant dose effects on biodistribution were detected, which might be a reflection of the study being underpowered to see these differences rather than a saturation effect at the lower dose. Additionally, in this study the volume of injection varied by route of administration. For direct cerebrospinal fluid injections, excessive volume can impede normal flow of cerebrospinal fluid or increase the intracranial/subarachnoid pressure, which may result in biodistribution effects [48,49]. We chose volumes that our group has used extensively in other studies and reported them in this study for transparency; however, determining how injection volume affects biodistribution was out of scope for this study.

The deaths observed in mice dosed P1 and P5 was most likely due to localized GFP overexpression toxicity. Most mice that died or needed to be euthanized were about 2 weeks post injection, which aligns with the typical timing of peak transgene expression from self-complementary AAV [10,50]. While GFP is typically well tolerated in mice, overexpression can be toxic and potentially immunogenic [51,52]. Similar doses of other transgenes delivered with AAV9 have been well tolerated in other studies at these young ages, including at higher doses, further implicating GFP-related toxicity rather than toxicity related to the AAV vector itself, route of administration, or treatment age [46,53,54]. However, taken together with other reports linking transgene overexpression from experimental gene therapy vectors to negative behavioral changes and toxicity [55–58], our data highlights the need for rigorous preclinical safety studies to rule out transgene toxicity due to overexpression. Overall, our conclusion is that the mice died from toxicity related to high localized transgene expression levels.

The primary goal of the study was to determine how routes of administration affected vector distribution in mouse tissue. Overall, our results suggest that direct CSF injection from IT, ICV, and IT & ICV routes of administration transduce CNS tissue better than a systemic IV injection at equivalent total vg doses, but do not substantially de-target peripheral tissue. AAV9 can cross the blood–brain barrier, so while the direct CSF routes help direct transduction in CNS tissue, vector will still be distributed throughout the body [40]. This was generally seen across all treatment ages assessed. The extensive peripheral tissue distribution from direct CSF administration matches other published studies, but it was somewhat surprising that there was little difference compared to IV administration, particularly with the liver. For example, while the IT biodistribution values at P28 matches earlier

studies from our lab [29], the IV biodistribution at P28 was markedly reduced compared to prior studies at similar doses [5,59]. Given the toxicity seen with GFP at P1 and P5, it is possible that there was subclinical GFP toxicity or immunogenicity in the highly transduced liver that reduced the vector DNA levels by the defined study endpoint. Beyond the liver, there were some notable differences in how the peripheral tissue was transduced by AAV9/GFP. Expression in muscle was high compared to all other peripheral tissues. AAV9 has been shown in the past to have a propensity to transduce cardiac and skeletal muscle to a high degree [34]. Additionally, high transgene expression in the heart driven by the CBh promoter has been previously reported [60].

The IT & ICV combination injection was included to determine if this dual route could provide added transduction benefit to either injection alone. We found that the IT & ICV injection was not additively better than the IT or ICV routes of administration alone. The combination did, however, offset the weaknesses of each singular route. Relative to IT alone, the combination increased brain transduction with little change in the spinal cord, and relative to ICV alone, the combination increased spinal cord transduction with little change in the brain.

While low numbers of histological samples prevented statistical analysis of the GFP immunohistochemistry, regional expression pattern differences were visually apparent. IT administration appears to produce an expression pattern stronger in the peripheral and caudal regions of the brain compared to ICV administration. This pattern is especially evident when comparing mice across the developmental timepoints, where by P28 less expression is seen in the subcortical areas of the brain compared to P1 and P5. Conversely, ICV administration tends to increase expression throughout the interior of the brain and hippocampus. Again, as mice are treated at older ages an expression pattern favoring the rostral regions of the brain is more apparent. Although not mechanistically evaluated here, one explanation for these pattern differences relates to CSF flow. CSF is produced in the choroid plexus of the cerebral ventricles and assumes a rostral to caudal unidirectional flow from the lateral to the third and fourth ventricles and exits into the subarachnoid space at the base of the brain. Once in the subarachnoid space, CSF flow becomes multidirectional around the spinal cord and through the central canal. This movement is mostly in a caudal direction on the ventral aspect of the spinal cord and rostral in direction on the dorsal aspect; however, random Brownian motion and areas of recirculation or vortices have also been reported [61]. Considering this, it is possible that viral vector administered via ICV administration to the lateral ventricle follows the natural flow of cerebrospinal fluid rostrally, while lumbar intrathecal administration flows less directly rostrally along the spinal cord to the brain. This would suggest an emerging trend across this study that the proximity of tissue to administration is a key factor in expression levels for AAV9/GFP. This hypothesis would account for the toxicity events noted previously, as well as regional brain and spinal cord expression patterns.

A secondary goal of the study was to determine how treatment age affected vector distribution in mice. While distribution differences are apparent when comparing early treatment ages—P1, P5, and P10—to later treatment P28, aligning with previous research, there are not many notable differences when comparing distribution across the early treatment ages, with a few exceptions, notably in the eye. P1, P5, and P10 were chosen because they are commonly used in gene therapy preclinical studies that target early intervention. Based on neurological features, roughly speaking a P1 mouse is equated to a preterm infant, a P5–10 mouse is equated to a full-term infant or toddler, and P28 is equated to a pre-pubescent child [62]. Many preclinical studies have adopted a P1 intervention, as it is the earliest postnatal timepoint for intervention. Our data argues that this should only be performed if there are biological/mechanistic reasons why that timepoint could be

important, since it overestimates the transduction efficiency that could be expected in a postnatal human, and thus underestimates a minimally effective dose.

Author Contributions: Conceptualization, M.R., A.B., and S.J.G.; investigation, M.R., A.B., S.P., and Y.H.; formal analysis, M.R. and A.B.; visualization, M.R. and A.B.; writing—original draft preparation, M.R. and A.B.; writing—review and editing, M.R., A.B., and S.J.G. All authors have read and agreed to the published version of the manuscript.

Funding: This research was funded by internal UT Southwestern Department of Pediatrics funds to SJG.

Institutional Review Board Statement: The animal study protocol was approved by the UT Southwestern Medical Center's Institutional Animal Care and Use Committee (protocol code 2018-102422; approval date 13 May 2024).

Informed Consent Statement: Not applicable.

Data Availability Statement: The data presented in this study are available on request from the corresponding author.

Acknowledgments: The viral vector was produced at the UNC Vector Core. We thank the UTSW Histo Pathology Core for paraffin processing. We thank the UTSW Whole Brain Microscopy Facility (RRID:SCR_017949) for the appropriate training and use of their Nanozoomer S60 (Hamamatsu Photonics, Japan). We thank the UTSW Neuro-Models Facility (RRID:SCR_022529) for providing the equipment and space required to perform the stereotaxic intracerebroventricular injections. We thank Mary Wight-Carter, DVM, DACVP for evaluating the histology slides for toxicity. We thank the UTSW Translational Gene Therapy Core for running the qPCR on their equipment.

Conflicts of Interest: The authors declare no conflicts of interest.

Abbreviations

The following abbreviations are used in this manuscript:

AAV9	Adeno-associated virus serotype 9
GFP	Green fluorescent protein
CNS	Central nervous system
CSF	Cerebrospinal fluid
IT	Intrathecal
ICV	Intracerebroventricular
IV	Intravenous
P	Postnatal day
H&E	Hematoxylin and eosin
IHC	Immunohistochemistry

Appendix A

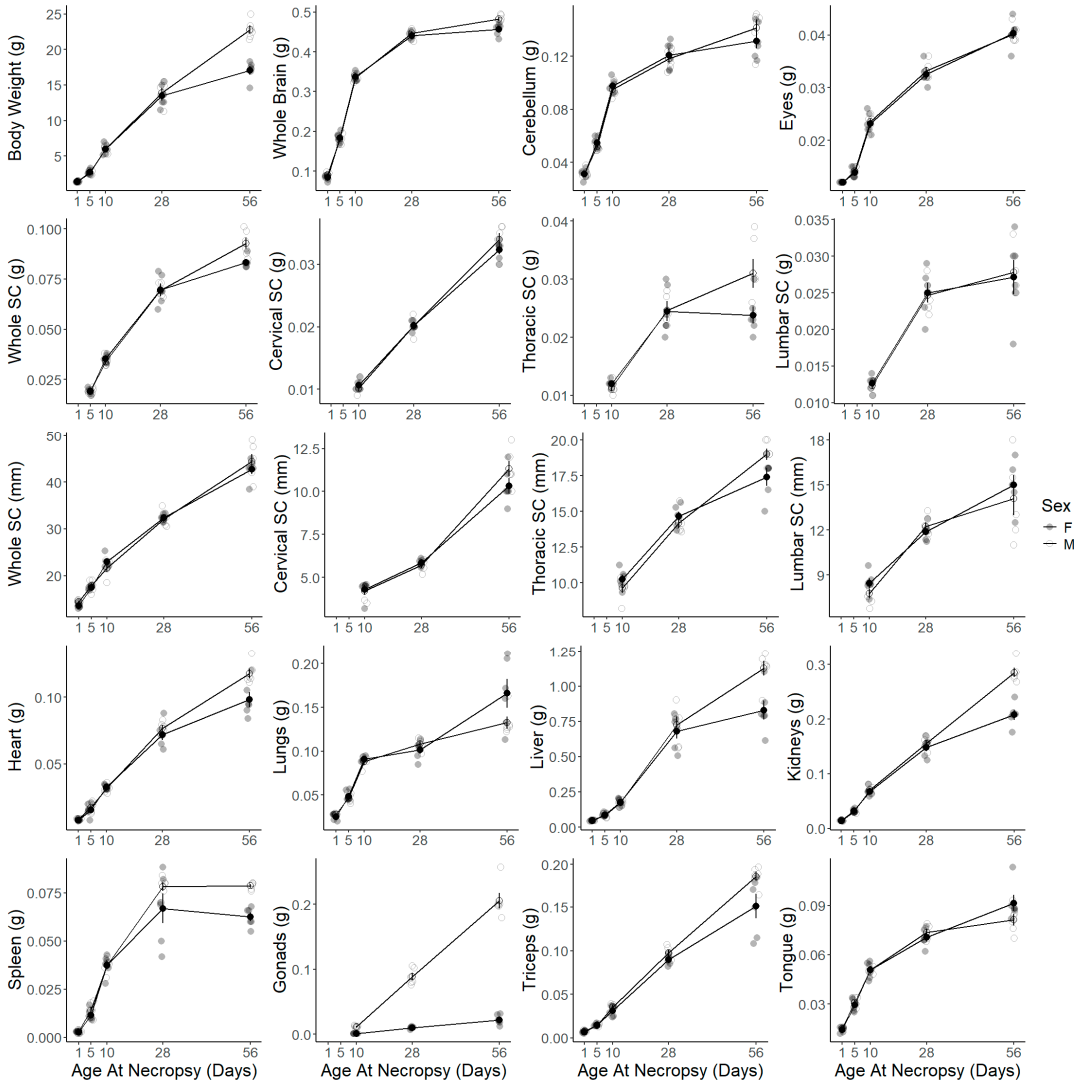

Figure A1. Organ growth of C57BL/6J male and female mice across development. First row: mouse body weight, whole brain weight, cerebellum weight, and left and right eye weight. Second row: whole spinal cord weight, followed by the weight of the spinal cord divided into cervical, thoracic, and lumbar sections. Third row: whole spinal cord length, followed by the length of the spinal cord divided into cervical, thoracic, and lumbar sections. Fourth row: heart, lung, liver, and left and right kidney weight. Fifth row: spleen, gonads, left and right triceps, and tongue weight. Mean and standard error for males (black open circle) and females (black closed circle) are included on each plot along with the individual mice (gray open and closed circles). The average values are listed in Table A1. SC = spinal cord. Error bars indicate standard error of the mean.

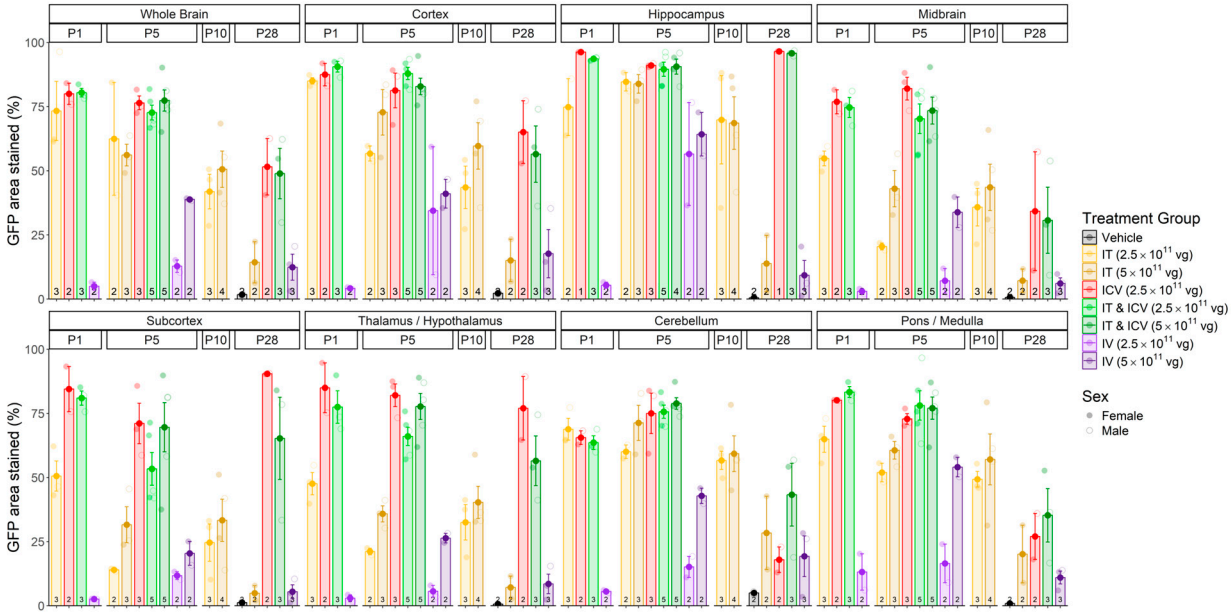

Figure A2. Expression of AAV9/GFP in brain regions. GFP expression was measured by percent DAB area stained by IHC in various brain regions for each treatment group after injection at P1, P5, P10, or P28. Brain areas assessed include whole brain, cortex, hippocampus, midbrain, subcortex, thalamus/hypothalamus, cerebellum, and pons/medulla. Error bars indicate standard error of the mean.

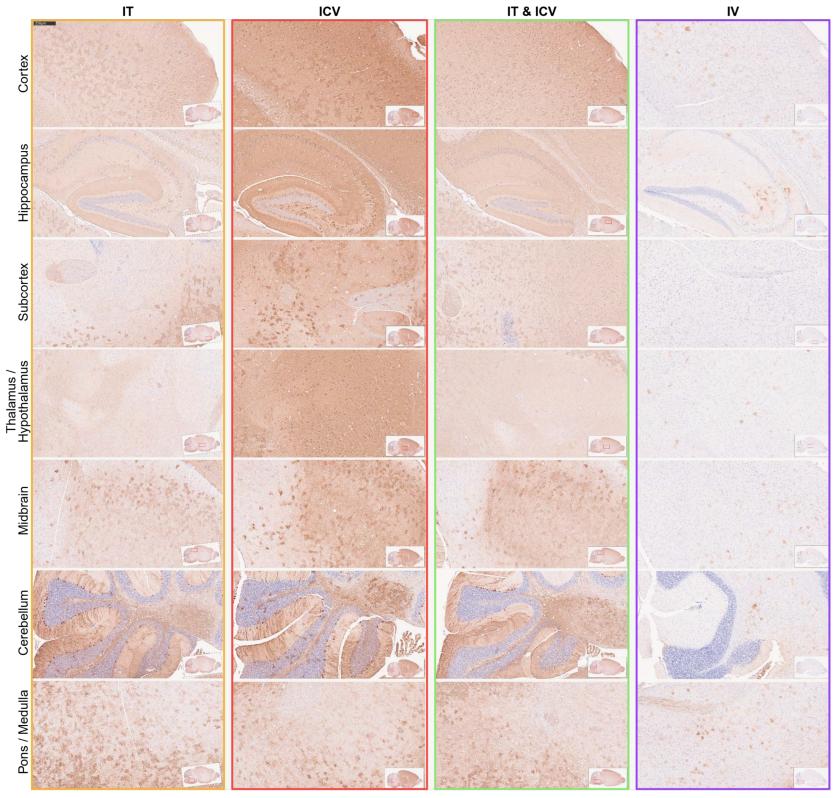

Figure A3. Expression of AAV9/GFP in brain regions after a P1 injection. Representative magnified images from Figure 2 of specific brain regions stained for GFP by IHC. Brain areas assessed include cortex, hippocampus, subcortex, thalamus/hypothalamus, midbrain, cerebellum, and pons/medulla. All images at 10× magnification, 250 µm scale bar. Location of magnified area within the whole brain shown in the lower right corner of each image.

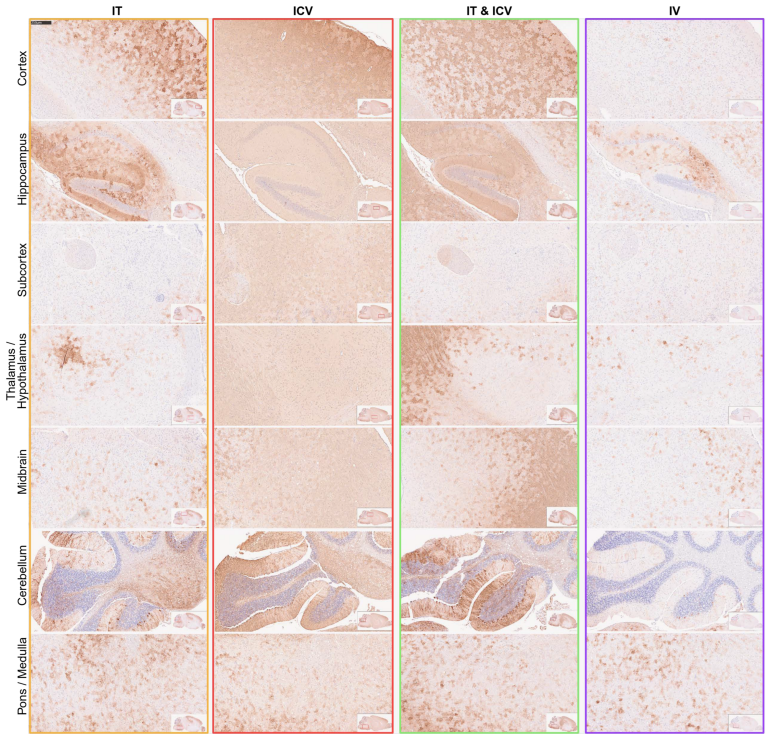

Figure A4. Expression of AAV9/GFP in brain regions after a P5 injection. Representative magnified images from Figure 2 of specific brain regions stained for GFP by IHC. Brain areas assessed include cortex, hippocampus, subcortex, thalamus/hypothalamus, midbrain, cerebellum, and pons/medulla. All images at 10× magnification, 250 µm scale bar. Location of magnified area within the whole brain shown in the lower right corner of each image.

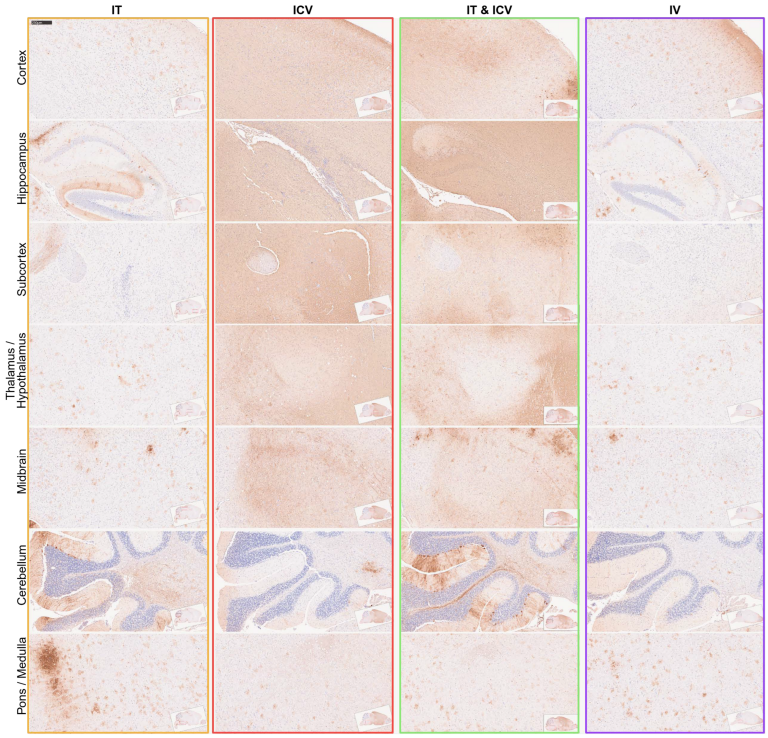

Figure A5. Expression of AAV9/GFP in brain regions after a P28 injection. Representative magnified images from Figure 2 of specific brain regions stained for GFP by IHC. Brain areas assessed include cortex, hippocampus, subcortex, thalamus/hypothalamus, midbrain, cerebellum, and pons/medulla. All images at 10× magnification, 250 µm scale bar. Location of magnified area within the whole brain shown in the lower right corner of each image.

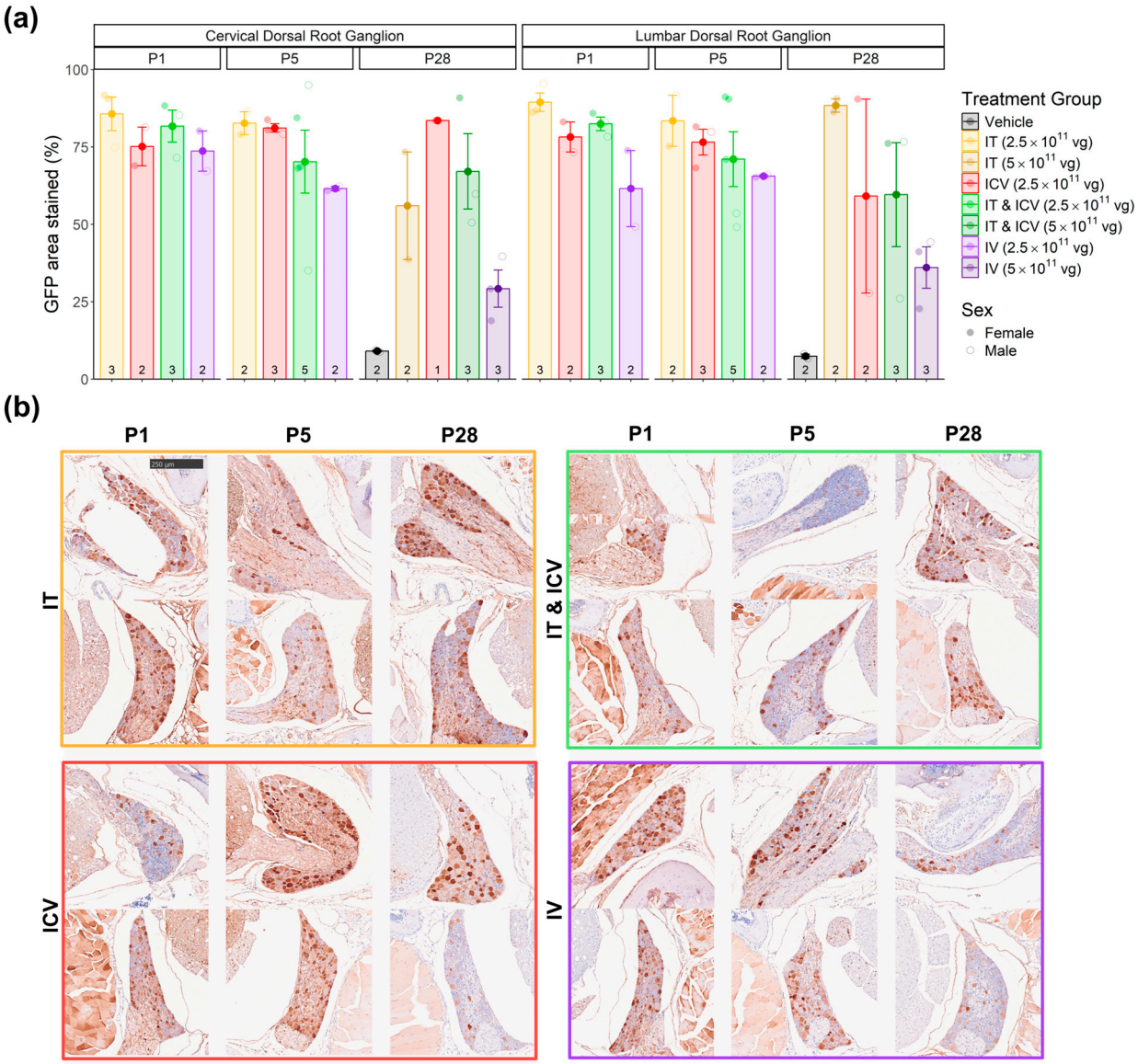

Figure A6. Expression of AAV9/GFP in the dorsal root ganglion. (**a**) GFP expression as measured by percent DAB area stained by IHC in the cervical and lumbar dorsal root ganglion for each treatment group after injection at P1, P5, or P28. Error bars indicate standard error of the mean. (**b**) Representative magnified images from Figure 3 of the cervical (**top**) and lumbar (**bottom**) dorsal root ganglion stained for GFP by IHC. All images at 10× magnification, 250 µm scale bar.

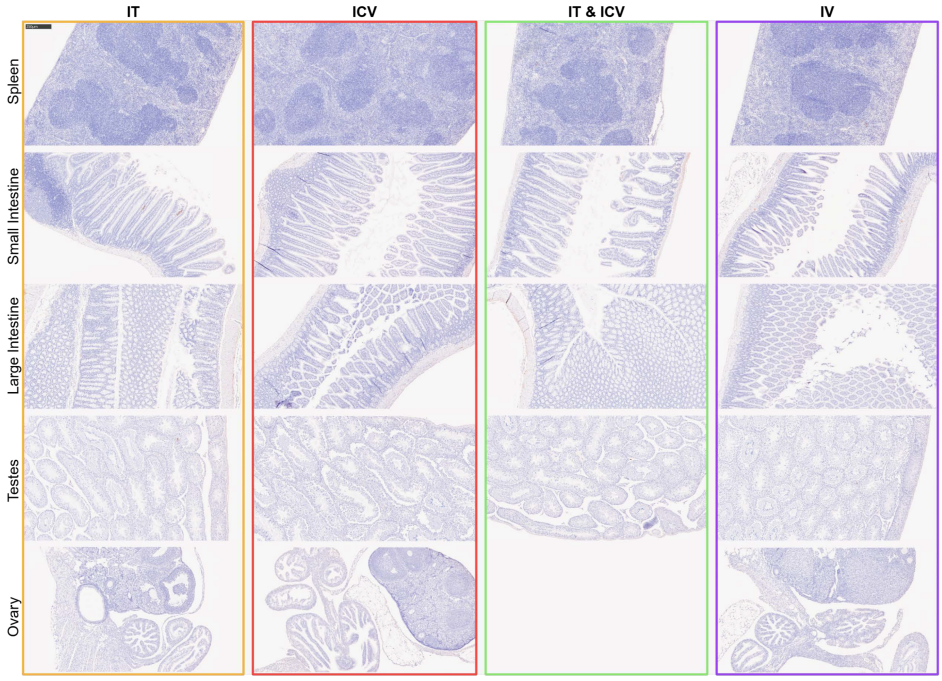

Figure A7. Expression of AAV9/GFP in additional peripheral tissues after a P1 injection. Representative magnified images were stained for GFP by IHC. Tissues assessed include spleen, small intestine, large intestine, ovary, and testes. All images at 10× magnification, 250 μm scale bar.

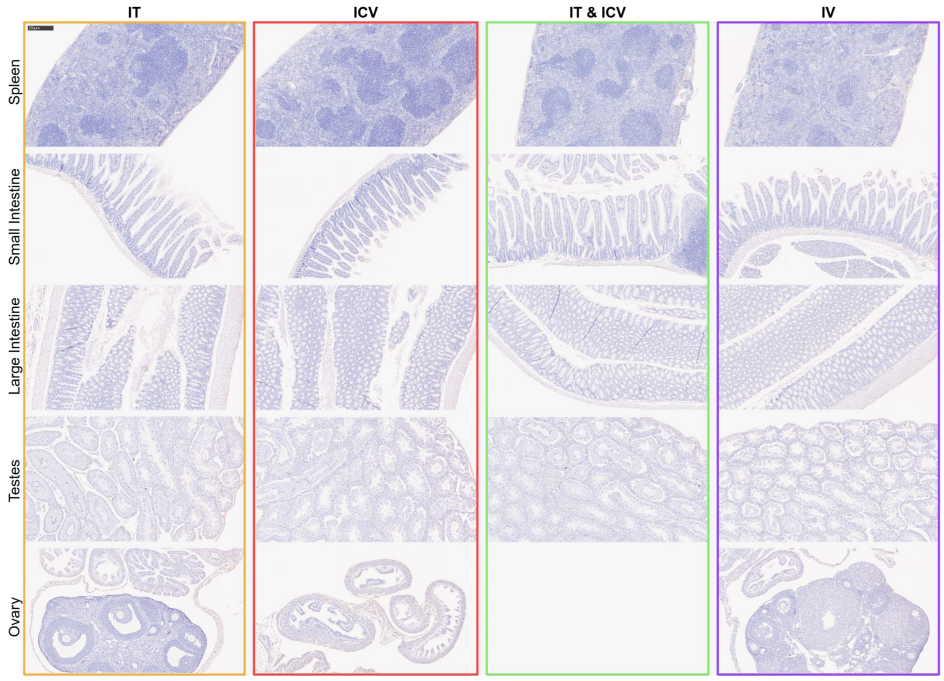

Figure A8. Expression of AAV9/GFP in additional peripheral tissues after a P5 injection. Representative magnified images were stained for GFP by IHC. Tissues assessed include spleen, small intestine, large intestine, ovary, and testes. All images at 10× magnification, 250 μm scale bar.

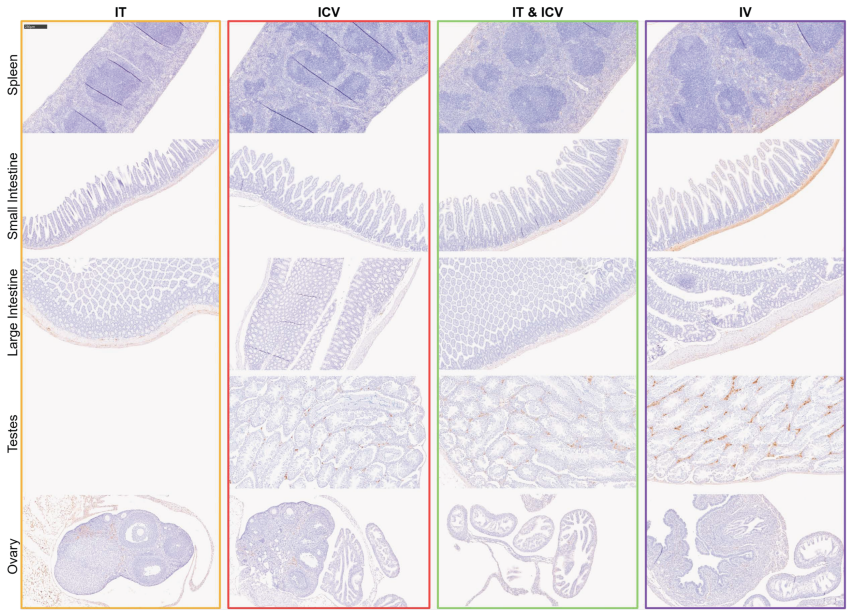

Figure A9. Expression of AAV9/GFP in additional peripheral tissues after a P28 injection. Representative magnified images were stained for GFP by IHC. Tissues assessed include spleen, small intestine, large intestine, ovary, and testes. All images at 10× magnification, 250 µm scale bar.

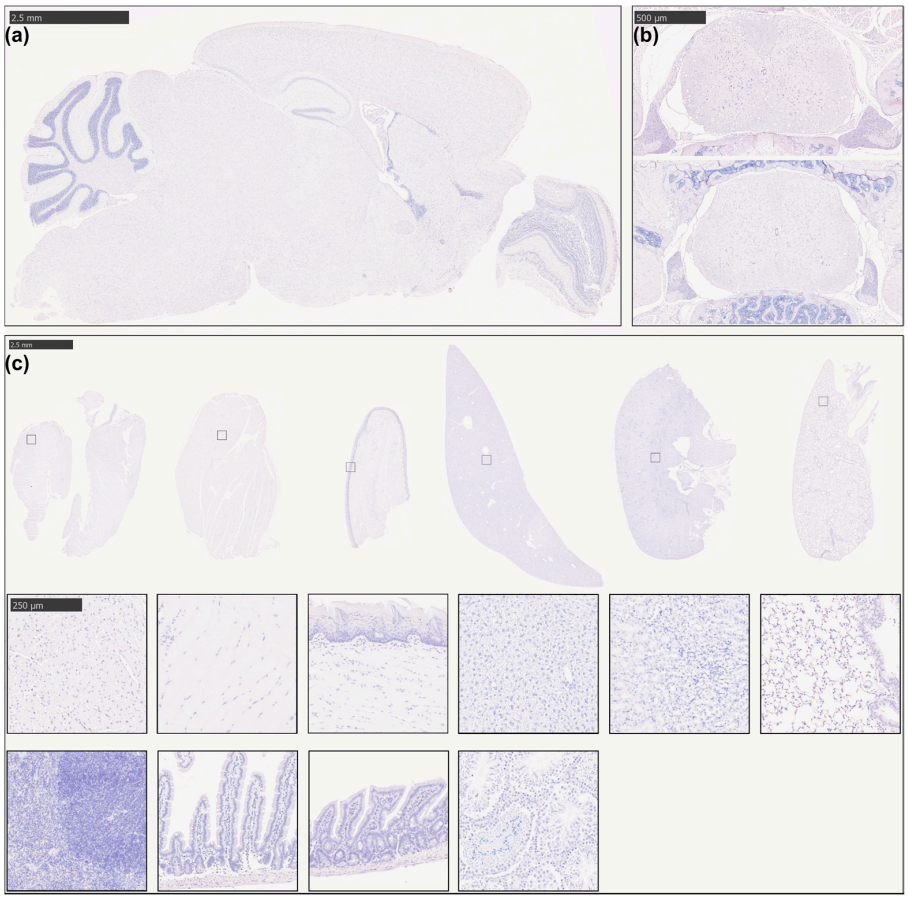

Figure A10. Representative GFP IHC vehicle control tissue. (**a**) Whole brain at 1.5× magnification, 2.5 mm scale bar. (**b**) Cervical (**top**) and lumbar (**bottom**) spinal cords with dorsal root ganglion at 5× magnification, 500 µm scale bar. (**c**) Peripheral tissue (top row): heart, triceps, tongue, liver, kidney, and lung (left to right) at 1.25× magnification, 2.5 mm scale bar, black squares show inset location. Magnified insets (middle row): heart, triceps, tongue, liver, kidney, lung and (bottom row): spleen, small intestine, large intestine, and testes (left to right). Insets at 10× magnification, 250 µm scale bar.

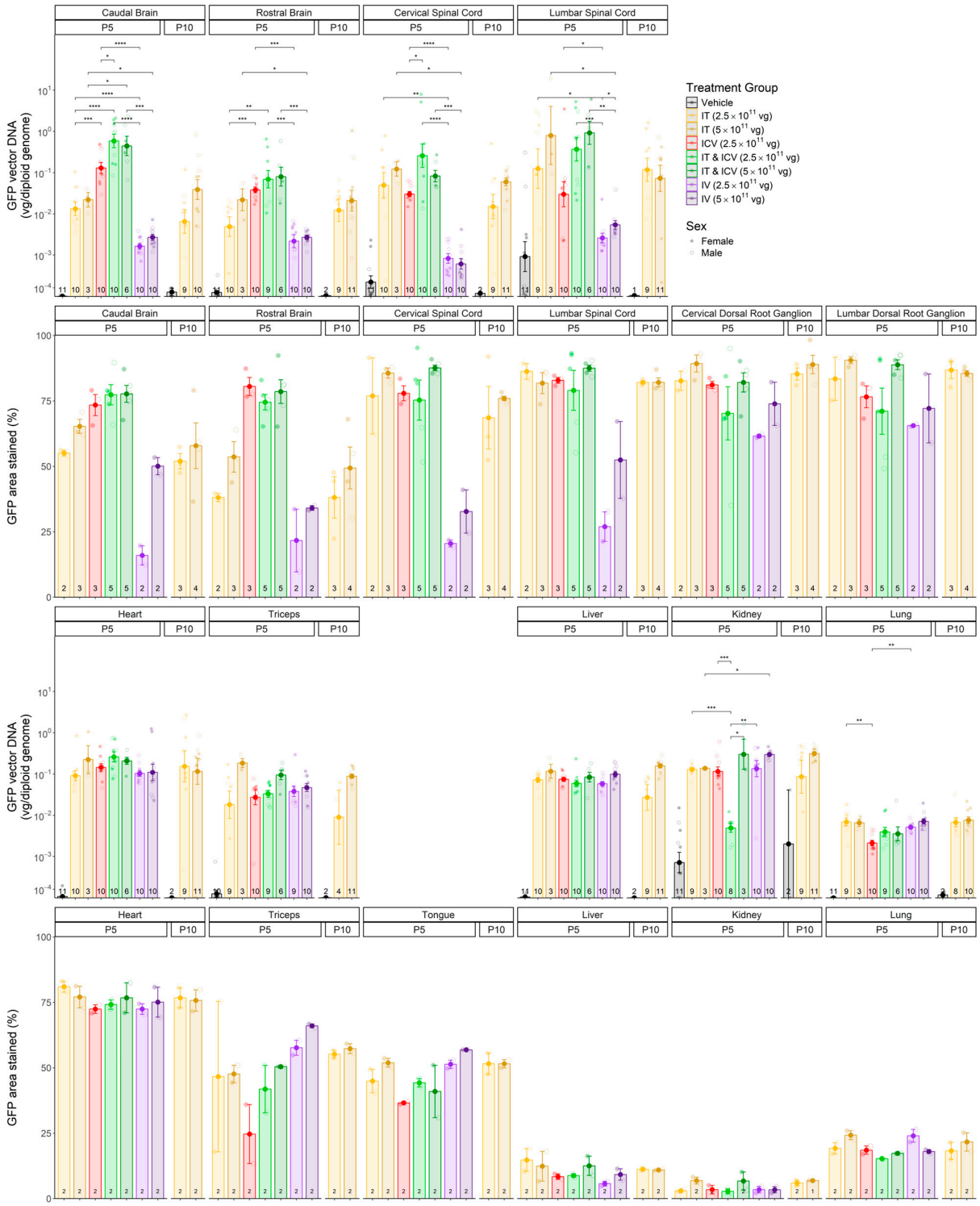

Figure A11. Expression of AAV9/GFP in CNS and peripheral tissues after injection at P5 or P10 to expand findings across additional ages and dose ranges. The data from the P5 2.5 × 10^{11} vg dose are the same as presented in the main text and are here for cross comparison with the P5 5 × 10^{11} vg dose and P10 data. GFP vector DNA as measured by qPCR (first and third rows) and GFP expression as measured by percent DAB area stained for GFP by IHC (second and fourth rows). Mean and standard error of the mean values for the GFP vector DNA plots are included in Table A3. The subset of samples for IHC analysis represent mice around the mean GFP vector DNA values across all tissues. * $0.01 < p \leq 0.05$, ** $0.001 < p \leq 0.01$, *** $0.0001 < p \leq 0.001$, **** $p \leq 0.0001$. Error bars indicate standard error of the mean.

Table A1. Organ growth of C57BL/6J male and female mice across development. The average weight and percent of P56 average weight or average length and percent of P56 average length were calculated for mouse organs at postnatal day 1, 5, 10, 28, and 56. Growth plots with averages are presented in Figure A1.

	Female					Male				
Age at Necropsy (Days)	**1**	**5**	**10**	**28**	**56**	**1**	**5**	**10**	**28**	**56**
Body Weight mean (g)	1.36	2.76	5.95	13.47	17.07	1.46	2.64	6.02	13.92	22.13
Body Weight mean (% of day 56 g)	8	16	35	79	100	6	12	26	61	100
Whole Brain mean (g)	0.084	0.184	0.337	0.441	0.457	0.090	0.181	0.335	0.446	0.482
Whole Brain (% of day 56 g)	18	40	74	97	100	19	38	70	93	100
Cerebellum mean (g)	0.031	0.055	0.098	0.121	0.132	0.032	0.052	0.095	0.118	0.142
Cerebellum (% of day 56 g)	24	42	74	92	100	22	37	67	84	100
Spinal Cord mean (g)		0.019	0.035	0.070	0.083		0.019	0.034	0.070	0.087
Spinal Cord mean (% of day 56 g)		23	42	84	100		20	37	75	100
Spinal Cord mean (mm)	13.55	17.34	22.99	32.38	42.75	14.47	17.83	21.59	32.11	46.42
Spinal Cord (% of day 56 mm)	32	41	54	76	100	31	38	47	69	100
Cervical SC mean (g)			0.011	0.020	0.032			0.010	0.020	0.034
Cervical SC (% of day 56 g)			33	62	100			29	59	100
Cervical SC mean (mm)			4.29	5.85	10.33			4.21	5.71	11.33
Cervical SC (% of day 56 mm)			42	57	100			37	50	100
Thoracic SC mean (g)			0.012	0.025	0.024			0.011	0.025	0.031
Thoracic SC (% of day 56 g)			50	103	100			35	80	100
Thoracic SC mean (mm)			10.25	14.65	17.42			9.62	14.18	19.00
Thoracic SC (% of day 56 mm)			59	84	100			51	75	100
Lumbar SC mean (g)			0.013	0.025	0.027			0.012	0.025	0.028
Lumbar SC (% of day 56 g)			47	92	100			43	89	100
Lumbar SC mean (mm)			8.45	11.89	15.00			7.77	12.23	14.1
Lumbar SC (% of day 56 mm)			56	79	100			55	86	100
Eyes mean (g)	0.012	0.014	0.023	0.033	0.040	0.012	0.014	0.024	0.033	0.040
Eyes (% of day 56 g)	30	35	57	81	100	30	35	60	83	100
Gonads mean (g)			0.001	0.010	0.022			0.012	0.089	0.206
Gonads (% of day 56 g)			5	45	100			6	43	100
Heart mean (g)	0.008	0.016	0.033	0.072	0.098	0.009	0.017	0.032	0.077	0.118
Heart (% of day 56 g)	8	16	33	73	100	8	14	27	65	100
Kidneys mean (g)	0.014	0.032	0.068	0.149	0.208	0.015	0.030	0.070	0.155	0.286
Kidneys (% of day 56 g)	7	16	33	71	100	5	10	24	54	100
Liver mean (g)	0.045	0.088	0.177	0.681	0.830	0.048	0.085	0.174	0.727	1.130
Liver (% of day 56 g)	5	11	21	82	100	4	8	15	64	100
Lungs mean (g)	0.025	0.049	0.091	0.102	0.166	0.028	0.047	0.088	0.108	0.133
Lungs mean (% of day 56 g)	15	30	55	61	100	21	35	66	81	100
Spleen mean (g)	0.003	0.012	0.038	0.067	0.063	0.003	0.014	0.037	0.078	0.064
Spleen (% of day 56 g)	4	19	60	107	100	5	22	58	122	100
Tongue mean (g)	0.015	0.029	0.051	0.071	0.092	0.015	0.031	0.051	0.074	0.081
Tongue (% of day 56 g)	16	32	55	77	100	19	38	63	91	100
Triceps mean (g)	0.007	0.015	0.031	0.090	0.151	0.008	0.015	0.035	0.098	0.185
Triceps (% of day 56 g)	5	10	21	59	100	4	8	19	53	100

Table A2. Pathological findings from euthanized mice due to toxicity. Peripheral organs include heart, lung, liver, kidney, spleen, skeletal muscle, small intestine, large intestine, and gonads unless separately indicated.

ID	Treatment Age	Route	Dose (vg)	Tissue	Results
41	P5	IT	5×10^{11}	Brain	Normal
				Heart	Right ventricular walls contained mild multifocal myocarditis with few degenerating myofibers and infiltrates with small numbers of inflammatory cells
				Peripheral Organs	Normal
				Dorsal Root Ganglion	Normal
				Cervical Spinal Cord	Normal
				Thoracic Spinal Cord	Diffuse Myelomalacia
				Lumbar Spinal Cord	Diffuse Myelomalacia
46	P5	IT and ICV	5×10^{11}	Brain	Focally extensive area in caudal thalamus contained mineralization of tissue that replaces normal neuropil. Scattered degenerating neurons and swollen axons in area adjacent to mineralized neuropil
				Peripheral Organs	Normal
				Dorsal Root Ganglion	Normal
				Cervical Spinal Cord	Diffuse degeneration-vacuolation of the dorsal tracts and central area with scattered degenerating neurons (Diffuse Myelomalacia)
				Thoracic Spinal Cord	Diffuse Myelomalacia
				Lumbar Spinal Cord	Mild, focal dorsolateral degeneration of gray matter
54	P5	IT and ICV	5×10^{11}	Brain	Cerebral cortex on one side of the brain contains swollen endothelial cells and multifocal perivascular infiltrates with small numbers of inflammatory cells with mild diffuse degeneration of neuropil and scattered degenerating neurons
				Peripheral Organs	Normal
				Dorsal Root Ganglion	Normal
				Cervical Spinal Cord	Normal
				Thoracic Spinal Cord	Normal
				Lumbar Spinal Cord	Diffuse Myelomalacia

Table A2. *Cont.*

ID	Treatment Age	Route	Dose (vg)	Tissue	Results
56	P5	IT	5×10^{11}	Brain	Olfactory bulb focal degeneration. Neuronal degeneration and few apoptotic cells
				Peripheral Organs	Normal
				Dorsal Root Ganglion	Normal
				Cervical Spinal Cord	Normal
				Thoracic Spinal Cord	Mild diffuse myelomalacia in gray matter
				Lumbar Spinal Cord	Diffuse Myelomalacia
58	P5	IT	5×10^{11}	Brain	Normal
				Liver	Diffuse lipidosis
				Peripheral Organs	Normal
				Dorsal Root Ganglion	Normal
				Cervical Spinal Cord	Mild focal ventrolateral myelomalacia
				Thoracic Spinal Cord	Diffuse Myelomalacia
				Lumbar Spinal Cord	Diffuse Myelomalacia
59	P5	IT	5×10^{11}	Brain	Normal
				Peripheral Organs	Normal
				Dorsal Root Ganglion	Normal
				Cervical Spinal Cord	Normal
				Thoracic Spinal Cord	Normal
				Lumbar Spinal Cord	Moderate unilateral myelomalacia
61	P5	IT	5×10^{11}	Brain	Normal
				Peripheral Organs	Normal
				Dorsal Root Ganglion	Normal
				Cervical Spinal Cord	Mild focal central myelomalacia
				Thoracic Spinal Cord	Diffuse myelomalacia
				Lumbar Spinal Cord	Diffuse Myelomalacia
84	P10	IT	5×10^{11}	Brain	Normal
				Peripheral Organs	Normal
				Dorsal Root Ganglion	Normal
				Cervical Spinal Cord	Diffuse myelomalacia
				Thoracic Spinal Cord	Diffuse myelomalacia
				Lumbar Spinal Cord	Diffuse myelomalacia

Table A3. AAV9/GFP vector genome biodistribution in the cerebrum, cerebellum, cervical spinal cord (CC), lumbar spinal cord (LC), heart, triceps, liver, kidney, and lung after injection at various treatment ages (P1, P5, P10, P28) and with various routes of administration (IT, ICV, IT & ICV, IV) and doses (2.5×10^{11}, 5×10^{11} vg). To provide benchmark values, the number of animals (n), mean GFP vg/diploid genome value, and standard error of the mean (SEM) from the data presented in Figures 2a, 3a, 4a and 5a, and A11 are included.

Tissue	Treatment Age	Treatment Group	n	Mean	SEM
Cerebrum	P1	Vehicle	8	4.32×10^{-6}	2.01×10^{-6}
Cerebrum	P1	IT (2.5×10^{11} vg)	8	0.102447	0.044186
Cerebrum	P1	ICV (2.5×10^{11} vg)	10	0.293985	0.069654
Cerebrum	P1	IT & ICV (2.5×10^{11} vg)	8	0.24631	0.129039
Cerebrum	P1	IV (2.5×10^{11} vg)	10	0.002756	0.000864
Cerebrum	P5	Vehicle	11	2.16×10^{-6}	1.5×10^{-6}
Cerebrum	P5	IT (2.5×10^{11} vg)	10	0.025329	0.010162
Cerebrum	P5	IT (5×10^{11} vg)	3	0.025431	0.008657
Cerebrum	P5	ICV (2.5×10^{11} vg)	10	0.194641	0.055924
Cerebrum	P5	IT & ICV (2.5×10^{11} vg)	10	0.956908	0.241648
Cerebrum	P5	IT & ICV (5×10^{11} vg)	6	0.82193	0.363852
Cerebrum	P5	IV (2.5×10^{11} vg)	10	0.001862	0.000318
Cerebrum	P5	IV (5×10^{11} vg)	10	0.003111	0.000581
Cerebrum	P10	Vehicle	2	5.14×10^{-5}	4.29×10^{-5}
Cerebrum	P10	IT (2.5×10^{11} vg)	9	0.022051	0.012492
Cerebrum	P10	IT (5×10^{11} vg)	10	0.141743	0.080822
Cerebrum	P28	Vehicle	8	2.77×10^{-5}	1.67×10^{-5}
Cerebrum	P28	IT (5×10^{11} vg)	10	0.019308	0.00951
Cerebrum	P28	ICV (2.5×10^{11} vg)	10	0.396319	0.295485
Cerebrum	P28	IT & ICV (5×10^{11} vg)	9	0.568634	0.310645
Cerebrum	P28	IV (5×10^{11} vg)	11	0.004638	0.001302
Cerebellum	P1	Vehicle	8	4.32×10^{-5}	2.02×10^{-5}
Cerebellum	P1	IT (2.5×10^{11} vg)	8	0.025478	0.00537
Cerebellum	P1	ICV (2.5×10^{11} vg)	9	0.047758	0.014028
Cerebellum	P1	IT & ICV (2.5×10^{11} vg)	8	0.111255	0.047246
Cerebellum	P1	IV (2.5×10^{11} vg)	10	0.008343	0.003263
Cerebellum	P5	Vehicle	11	5.04×10^{-5}	2.62×10^{-5}
Cerebellum	P5	IT (2.5×10^{11} vg)	10	0.009729	0.002266
Cerebellum	P5	IT (5×10^{11} vg)	3	0.029999	0.014376
Cerebellum	P5	ICV (2.5×10^{11} vg)	10	0.04318	0.006958
Cerebellum	P5	IT & ICV (2.5×10^{11} vg)	9	0.165604	0.074651
Cerebellum	P5	IT & ICV (5×10^{11} vg)	6	0.15889	0.087587
Cerebellum	P5	IV (2.5×10^{11} vg)	10	0.00322	0.000708
Cerebellum	P5	IV (5×10^{11} vg)	10	0.002878	0.000312
Cerebellum	P10	Vehicle	2	9.99×10^{-6}	9.81×10^{-6}
Cerebellum	P10	IT (2.5×10^{11} vg)	9	0.023651	0.006325
Cerebellum	P10	IT (5×10^{11} vg)	11	0.127843	0.092515
Cerebellum	P28	Vehicle	8	9.33×10^{-5}	4.13×10^{-5}
Cerebellum	P28	IT (5×10^{11} vg)	10	0.010536	0.004947
Cerebellum	P28	ICV (2.5×10^{11} vg)	10	0.00397	0.000673
Cerebellum	P28	IT & ICV (5×10^{11} vg)	9	0.033399	0.025375
Cerebellum	P28	IV (5×10^{11} vg)	11	0.001779	0.000412
CC	P1	Vehicle	8	0.000117	4.75×10^{-5}
CC	P1	IT (2.5×10^{11} vg)	8	0.398777	0.240798
CC	P1	ICV (2.5×10^{11} vg)	10	0.065529	0.016879
CC	P1	IT & ICV (2.5×10^{11} vg)	8	0.04707	0.009463
CC	P1	IV (2.5×10^{11} vg)	10	0.007333	0.001413
CC	P5	Vehicle	11	0.000423	0.000237

Table A3. *Cont.*

Tissue	Treatment Age	Treatment Group	n	Mean	SEM
CC	P5	IT (2.5×10^{11} vg)	10	0.165295	0.07528
CC	P5	IT (5×10^{11} vg)	3	0.140197	0.042674
CC	P5	ICV (2.5×10^{11} vg)	10	0.033547	0.005325
CC	P5	IT & ICV (2.5×10^{11} vg)	10	1.464239	0.867967
CC	P5	IT & ICV (5×10^{11} vg)	6	0.109702	0.038902
CC	P5	IV (2.5×10^{11} vg)	10	0.001126	0.000288
CC	P5	IV (5×10^{11} vg)	10	0.000964	0.000392
CC	P10	Vehicle	2	0.000035	1.56×10^{-5}
CC	P10	IT (2.5×10^{11} vg)	9	0.076517	0.054427
CC	P10	IT (5×10^{11} vg)	11	0.072333	0.011598
CC	P28	Vehicle	8	0.000116	4.17×10^{-5}
CC	P28	IT (5×10^{11} vg)	10	0.027687	0.00703
CC	P28	ICV (2.5×10^{11} vg)	10	0.009873	0.00235
CC	P28	IT & ICV (5×10^{11} vg)	10	0.025273	0.006746
CC	P28	IV (5×10^{11} vg)	11	0.00362	0.000649
LC	P1	Vehicle	8	0.000439	0.000271
LC	P1	IT (2.5×10^{11} vg)	8	0.129227	0.049089
LC	P1	ICV (2.5×10^{11} vg)	8	0.098964	0.010218
LC	P1	IT & ICV (2.5×10^{11} vg)	5	0.091337	0.035106
LC	P1	IV (2.5×10^{11} vg)	10	0.004071	0.000715
LC	P5	Vehicle	11	0.032544	0.02752
LC	P5	IT (2.5×10^{11} vg)	9	0.924787	0.396028
LC	P5	IT (5×10^{11} vg)	3	6.511957	6.325121
LC	P5	ICV (2.5×10^{11} vg)	10	0.37731	0.343337
LC	P5	IT & ICV (2.5×10^{11} vg)	10	1.427414	0.593922
LC	P5	IT & ICV (5×10^{11} vg)	6	1.9664	0.887217
LC	P5	IV (2.5×10^{11} vg)	10	0.004237	0.00206
LC	P5	IV (5×10^{11} vg)	10	0.007964	0.003409
LC	P10	Vehicle	1	1.09×10^{-5}	
LC	P10	IT (2.5×10^{11} vg)	9	0.414056	0.194415
LC	P10	IT (5×10^{11} vg)	11	0.209608	0.062819
LC	P28	Vehicle	8	0.012399	0.012347
LC	P28	IT (5×10^{11} vg)	10	0.205819	0.092671
LC	P28	ICV (2.5×10^{11} vg)	10	0.008841	0.002368
LC	P28	IT & ICV (5×10^{11} vg)	10	0.073904	0.012392
LC	P28	IV (5×10^{11} vg)	11	0.317236	0.290775
Heart	P1	Vehicle	8	8.92×10^{-6}	2.61×10^{-6}
Heart	P1	IT (2.5×10^{11} vg)	8	0.052463	0.017924
Heart	P1	ICV (2.5×10^{11} vg)	10	0.049528	0.013217
Heart	P1	IT & ICV (2.5×10^{11} vg)	8	0.120476	0.054282
Heart	P1	IV (2.5×10^{11} vg)	9	0.075144	0.02449
Heart	P5	Vehicle	11	1.7×10^{-5}	1.32×10^{-5}
Heart	P5	IT (2.5×10^{11} vg)	10	0.154575	0.077782
Heart	P5	IT (5E11 vg)	3	0.422556	0.318635
Heart	P5	ICV (2.5×10^{11} vg)	10	0.17524	0.037998
Heart	P5	IT & ICV (2.5×10^{11} vg)	10	0.358254	0.087475
Heart	P5	IT & ICV (5×10^{11} vg)	6	0.225698	0.038377
Heart	P5	IV (2.5×10^{11} vg)	10	0.117282	0.022451
Heart	P5	IV (5×10^{11} vg)	10	0.294602	0.145772
Heart	P10	Vehicle	2	2.08×10^{-6}	1.1×10^{-6}
Heart	P10	IT (2.5×10^{11} vg)	9	0.717027	0.342695
Heart	P10	IT (5×10^{11} vg)	11	0.255926	0.067512

Table A3. *Cont.*

Tissue	Treatment Age	Treatment Group	n	Mean	SEM
Heart	P28	Vehicle	8	3.02×10^{-5}	1.66×10^{-5}
Heart	P28	IT (5×10^{11} vg)	10	0.740474	0.607256
Heart	P28	ICV (2.5×10^{11} vg)	10	0.048292	0.010894
Heart	P28	IT & ICV (5×10^{11} vg)	10	0.093108	0.026359
Heart	P28	IV (5×10^{11} vg)	11	0.112665	0.029511
Triceps	P1	Vehicle	8	3.51×10^{-5}	1.99×10^{-5}
Triceps	P1	IT (2.5×10^{11} vg)	8	0.068784	0.022383
Triceps	P1	ICV (2.5×10^{11} vg)	9	0.067039	0.009529
Triceps	P1	IT & ICV (2.5×10^{11} vg)	6	0.059233	0.010782
Triceps	P1	IV (2.5×10^{11} vg)	9	0.12769	0.041284
Triceps	P5	Vehicle	10	8.06×10^{-5}	7.41×10^{-5}
Triceps	P5	IT (2.5×10^{11} vg)	9	0.051223	0.01778
Triceps	P5	IT (5×10^{11} vg)	3	0.197105	0.050933
Triceps	P5	ICV (2.5×10^{11} vg)	10	0.039168	0.006219
Triceps	P5	IT & ICV (2.5×10^{11} vg)	9	0.038521	0.006767
Triceps	P5	IT & ICV (5×10^{11} vg)	6	0.11019	0.022873
Triceps	P5	IV (2.5×10^{11} vg)	9	0.061003	0.029511
Triceps	P5	IV (5×10^{11} vg)	10	0.056974	0.010734
Triceps	P10	Vehicle	2	2.88×10^{-6}	2.06×10^{-6}
Triceps	P10	IT (2.5×10^{11} vg)	4	0.032245	0.013174
Triceps	P10	IT (5×10^{11} vg)	11	0.095756	0.011611
Triceps	P28	Vehicle	8	0.001022	0.000898
Triceps	P28	IT (5×10^{11} vg)	10	0.08322	0.029194
Triceps	P28	ICV (2.5×10^{11} vg)	10	0.017735	0.004276
Triceps	P28	IT & ICV (5×10^{11} vg)	10	0.022359	0.00308
Triceps	P28	IV (5×10^{11} vg)	11	0.066568	0.01349
Liver	P1	Vehicle	8	0.000157	0.000119
Liver	P1	IT (2.5×10^{11} vg)	8	0.035159	0.008029
Liver	P1	ICV (2.5×10^{11} vg)	10	0.049701	0.008447
Liver	P1	IT & ICV (2.5×10^{11} vg)	8	0.040964	0.010355
Liver	P1	IV (2.5×10^{11} vg)	10	0.068126	0.006556
Liver	P5	Vehicle	11	9.93×10^{-6}	5.92×10^{-6}
Liver	P5	IT (2.5×10^{11} vg)	10	0.078141	0.008971
Liver	P5	IT (5×10^{11} vg)	3	0.136628	0.05648
Liver	P5	ICV (2.5×10^{11} vg)	10	0.079413	0.009183
Liver	P5	IT & ICV (2.5×10^{11} vg)	10	0.071407	0.018725
Liver	P5	IT & ICV (5×10^{11} vg)	6	0.098432	0.021792
Liver	P5	IV (2.5×10^{11} vg)	10	0.061981	0.007261
Liver	P5	IV (5×10^{11} vg)	10	0.110948	0.016976
Liver	P10	Vehicle	2	8.22×10^{-7}	7.98×10^{-7}
Liver	P10	IT (2.5×10^{11} vg)	9	0.052323	0.009476
Liver	P10	IT (5×10^{11} vg)	11	0.168115	0.01815
Liver	P28	Vehicle	8	0.000353	0.000195
Liver	P28	IT (5×10^{11} vg)	10	2.051217	0.378247
Liver	P28	ICV (2.5×10^{11} vg)	10	0.905311	0.213485
Liver	P28	IT & ICV (5×10^{11} vg)	10	3.94184	0.512413
Liver	P28	IV (5×10^{11} vg)	11	2.012641	0.404079
Kidney	P1	Vehicle	8	0.007905	0.005895
Kidney	P1	IT (2.5×10^{11} vg)	8	0.074615	0.019832
Kidney	P1	ICV (2.5×10^{11} vg)	10	0.138964	0.019155
Kidney	P1	IT & ICV (2.5×10^{11} vg)	8	0.175971	0.023691
Kidney	P1	IV (2.5×10^{11} vg)	10	0.084577	0.005508

Table A3. *Cont.*

Tissue	Treatment Age	Treatment Group	n	Mean	SEM
Kidney	P5	Vehicle	11	0.002789	0.001392
Kidney	P5	IT (2.5×10^{11} vg)	9	0.135102	0.013184
Kidney	P5	IT (5×10^{11} vg)	3	0.138207	0.003751
Kidney	P5	ICV (2.5×10^{11} vg)	10	0.162794	0.054997
Kidney	P5	IT & ICV (2.5×10^{11} vg)	8	0.005887	0.001175
Kidney	P5	IT & ICV (5×10^{11} vg)	3	0.628268	0.498881
Kidney	P5	IV (2.5×10^{11} vg)	10	0.207261	0.04166
Kidney	P5	IV (5×10^{11} vg)	10	0.305284	0.023679
Kidney	P10	Vehicle	2	0.020614	0.020614
Kidney	P10	IT (2.5×10^{11} vg)	9	0.247392	0.055862
Kidney	P10	IT (5×10^{11} vg)	11	0.331744	0.033249
Kidney	P28	Vehicle	7	0.019456	0.010574
Kidney	P28	IT (5×10^{11} vg)	10	0.3278	0.045497
Kidney	P28	ICV (2.5×10^{11} vg)	10	0.107466	0.01345
Kidney	P28	IT & ICV (5×10^{11} vg)	10	0.247028	0.036241
Kidney	P28	IV (5×10^{11} vg)	10	0.305606	0.056409
Lung	P1	Vehicle	8	1.43×10^{-7}	5.13×10^{-8}
Lung	P1	IT (2.5×10^{11} vg)	8	0.00458	0.001143
Lung	P1	ICV (2.5×10^{11} vg)	10	0.004342	0.000904
Lung	P1	IT & ICV (2.5×10^{11} vg)	8	0.005858	0.000636
Lung	P1	IV (2.5×10^{11} vg)	9	0.005522	0.001366
Lung	P5	Vehicle	11	1.2×10^{-7}	5.68×10^{-8}
Lung	P5	IT (2.5×10^{11} vg)	9	0.008242	0.001618
Lung	P5	IT (5×10^{11} vg)	3	0.006844	0.001357
Lung	P5	ICV (2.5×10^{11} vg)	10	0.00238	0.000398
Lung	P5	IT & ICV (2.5×10^{11} vg)	9	0.005243	0.001521
Lung	P5	IT & ICV (5×10^{11} vg)	6	0.005913	0.003387
Lung	P5	IV (2.5×10^{11} vg)	10	0.005337	0.000451
Lung	P5	IV (5×10^{11} vg)	10	0.007994	0.001487
Lung	P10	Vehicle	2	3.33×10^{-5}	3.33×10^{-5}
Lung	P10	IT (2.5×10^{11} vg)	8	0.009047	0.003346
Lung	P10	IT (5×10^{11} vg)	10	0.008969	0.00185
Lung	P28	Vehicle	8	2.27×10^{-6}	1.99×10^{-6}
Lung	P28	IT (5×10^{11} vg)	9	0.016332	0.013837
Lung	P28	ICV (2.5×10^{11} vg)	9	0.00052	7.45×10^{-5}
Lung	P28	IT & ICV (5×10^{11} vg)	7	0.001953	0.000371
Lung	P28	IV (5×10^{11} vg)	10	0.002637	0.000422

References

1. Duque, S.; Joussemet, B.; Riviere, C.; Marais, T.; Dubreil, L.; Douar, A.M.; Fyfe, J.; Moullier, P.; Colle, M.A.; Barkats, M. Intravenous administration of self-complementary AAV9 enables transgene delivery to adult motor neurons. *Mol. Ther.* **2009**, *17*, 1187–1196. [CrossRef]
2. Foust, K.D.; Nurre, E.; Montgomery, C.L.; Hernandez, A.; Chan, C.M.; Kaspar, B.K. Intravascular AAV9 preferentially targets neonatal neurons and adult astrocytes. *Nat. Biotechnol.* **2009**, *27*, 59–65. [CrossRef]
3. Miyake, N.; Miyake, K.; Yamamoto, M.; Hirai, Y.; Shimada, T. Global gene transfer into the CNS across the BBB after neonatal systemic delivery of single-stranded AAV vectors. *Brain Res.* **2011**, *1389*, 19–26. [CrossRef] [PubMed]
4. Bevan, A.K.; Duque, S.; Foust, K.D.; Morales, P.R.; Braun, L.; Schmelzer, L.; Chan, C.M.; McCrate, M.; Chicoine, L.G.; Coley, B.D.; et al. Systemic gene delivery in large species for targeting spinal cord, brain, and peripheral tissues for pediatric disorders. *Mol. Ther.* **2011**, *19*, 1971–1980. [CrossRef]
5. Gray, S.J.; Matagne, V.; Bachaboina, L.; Yadav, S.; Ojeda, S.R.; Samulski, R.J. Preclinical differences of intravascular AAV9 delivery to neurons and glia: A comparative study of adult mice and nonhuman primates. *Mol. Ther.* **2011**, *19*, 1058–1069. [CrossRef] [PubMed]

6. Gao, G.; Vandenberghe, L.H.; Alvira, M.R.; Lu, Y.; Calcedo, R.; Zhou, X.; Wilson, J.M. Clades of Adeno-associated viruses are widely disseminated in human tissues. *J. Virol.* **2004**, *78*, 6381–6388. [CrossRef]
7. Ballon, D.J.; Rosenberg, J.B.; Fung, E.K.; Nikolopoulou, A.; Kothari, P.; De, B.P.; He, B.; Chen, A.; Heier, L.A.; Sondhi, D.; et al. Quantitative Whole-Body Imaging of I-124-Labeled Adeno-Associated Viral Vector Biodistribution in Nonhuman Primates. *Hum. Gene Ther.* **2020**, *31*, 1237–1259. [CrossRef] [PubMed]
8. Meadows, A.S.; Pineda, R.J.; Goodchild, L.; Bobo, T.A.; Fu, H. Threshold for Pre-existing Antibody Levels Limiting Transduction Efficiency of Systemic rAAV9 Gene Delivery: Relevance for Translation. *Mol. Ther. Methods Clin. Dev.* **2019**, *13*, 453–462. [CrossRef]
9. Murrey, D.A.; Naughton, B.J.; Duncan, F.J.; Meadows, A.S.; Ware, T.A.; Campbell, K.J.; Bremer, W.G.; Walker, C.M.; Goodchild, L.; Bolon, B.; et al. Feasibility and safety of systemic rAAV9-hNAGLU delivery for treating mucopolysaccharidosis IIIB: Toxicology, biodistribution, and immunological assessments in primates. *Hum. Gene Ther. Clin. Dev.* **2014**, *25*, 72–84. [CrossRef]
10. McCarty, D.M. Self-complementary AAV vectors; advances and applications. *Mol. Ther.* **2008**, *16*, 1648–1656. [CrossRef]
11. Wang, J.H.; Gessler, D.J.; Zhan, W.; Gallagher, T.L.; Gao, G. Adeno-associated virus as a delivery vector for gene therapy of human diseases. *Signal Transduct. Target. Ther.* **2024**, *9*, 78. [CrossRef] [PubMed]
12. Powell, S.K.; Rivera-Soto, R.; Gray, S.J. Viral expression cassette elements to enhance transgene target specificity and expression in gene therapy. *Discov. Med.* **2015**, *19*, 49–57.
13. Castle, M.J.; Cheng, Y.; Asokan, A.; Tuszynski, M.H. Physical positioning markedly enhances brain transduction after intrathecal AAV9 infusion. *Sci. Adv.* **2018**, *4*, eaau9859. [CrossRef]
14. Daci, R.; Flotte, T.R. Delivery of Adeno-Associated Virus Vectors to the Central Nervous System for Correction of Single Gene Disorders. *Int. J. Mol. Sci.* **2024**, *25*, 1050. [CrossRef]
15. Zhou, K.; Han, J.; Wang, Y.; Zhang, Y.; Zhu, C. Routes of administration for adeno-associated viruses carrying gene therapies for brain diseases. *Front. Mol. Neurosci.* **2022**, *15*, 988914. [CrossRef]
16. Chen, X.; Lim, D.A.; Lawlor, M.W.; Dimmock, D.; Vite, C.H.; Lester, T.; Tavakkoli, F.; Sadhu, C.; Prasad, S.; Gray, S.J. Biodistribution of Adeno-Associated Virus Gene Therapy Following Cerebrospinal Fluid-Directed Administration. *Hum. Gene Ther.* **2023**, *34*, 94–111. [CrossRef]
17. Garza, I.T.; Eller, M.M.; Holmes, S.K.; Schackmuth, M.K.; Bailey, R.M. Expression and distribution of rAAV9 intrathecally administered in juvenile to adolescent mice. *Gene Ther.* **2025**, *32*, 189–196. [CrossRef]
18. BioMarin Pharmaceutical Inc. ROCTAVIAN (Valoctocogene Roxaparvovec-Rvox) Prescribing Information. Available online: https://www.fda.gov/vaccines-blood-biologics/roctavian (accessed on 2 December 2025).
19. CSL Behring LLC. HEMGENIX (Etranacogene Dezaparvovec-Drlb) Prescribing Information. Available online: https://www.fda.gov/vaccines-blood-biologics/vaccines/hemgenix (accessed on 2 December 2025).
20. Novartis Gene Therapies Inc. ZOLGENSMA® (Onasemnogene Abeparvovec-Xioi) Prescribing Information. Available online: https://www.fda.gov/vaccines-blood-biologics/zolgensma (accessed on 2 December 2025).
21. Pfizer Inc. BEQVEZTM (Fidanacogene Elaparvovec-Dzkt) Prescribing Information. Available online: https://www.fda.gov/vaccines-blood-biologics/cellular-gene-therapy-products/beqvez (accessed on 2 December 2025).
22. Sarepta Therapeutics Inc. ELEVIDYS (Delandistrogene Moxeparvovec-Rokl) Prescribing Information. Available online: https://www.fda.gov/vaccines-blood-biologics/tissue-tissue-products/elevidys (accessed on 2 December 2025).
23. Yao, Y.; Wang, J.; Liu, Y.; Qu, Y.; Wang, K.; Zhang, Y.; Chang, Y.; Yang, Z.; Wan, J.; Liu, J.; et al. Variants of the adeno-associated virus serotype 9 with enhanced penetration of the blood-brain barrier in rodents and primates. *Nat. Biomed. Eng.* **2022**, *6*, 1257–1271. [CrossRef]
24. Federici, T.; Taub, J.S.; Baum, G.R.; Gray, S.J.; Grieger, J.C.; Matthews, K.A.; Handy, C.R.; Passini, M.A.; Samulski, R.J.; Boulis, N.M. Robust spinal motor neuron transduction following intrathecal delivery of AAV9 in pigs. *Gene Ther.* **2012**, *19*, 852–859. [CrossRef] [PubMed]
25. Schuster, D.J.; Dykstra, J.A.; Riedl, M.S.; Kitto, K.F.; Belur, L.R.; McIvor, R.S.; Elde, R.P.; Fairbanks, C.A.; Vulchanova, L. Biodistribution of adeno-associated virus serotype 9 (AAV9) vector after intrathecal and intravenous delivery in mouse. *Front. Neuroanat.* **2014**, *8*, 42. [CrossRef] [PubMed]
26. Novartis Gene Therapies Inc. ITVISMA® (Onasemnogene Abeparvovec-Brve) Prescribing Information. Available online: https://www.fda.gov/vaccines-blood-biologics/cellular-gene-therapy-products/itvisma (accessed on 2 December 2025).
27. Belur, L.R.; Romero, M.; Lee, J.; Podetz-Pedersen, K.M.; Nan, Z.; Riedl, M.S.; Vulchanova, L.; Kitto, K.F.; Fairbanks, C.A.; Kozarsky, K.F.; et al. Comparative Effectiveness of Intracerebroventricular, Intrathecal, and Intranasal Routes of AAV9 Vector Administration for Genetic Therapy of Neurologic Disease in Murine Mucopolysaccharidosis Type I. *Front. Mol. Neurosci.* **2021**, *14*, 618360. [CrossRef] [PubMed]
28. Bey, K.; Deniaud, J.; Dubreil, L.; Joussemet, B.; Cristini, J.; Ciron, C.; Hordeaux, J.; Le Boulc'h, M.; Marche, K.; Maquigneau, M.; et al. Intra-CSF AAV9 and AAVrh10 Administration in Nonhuman Primates: Promising Routes and Vectors for Which Neurological Diseases? *Mol. Ther. Methods Clin. Dev.* **2020**, *17*, 771–784. [CrossRef]

29. Bailey, R.M.; Rozenberg, A.; Gray, S.J. Comparison of high-dose intracisterna magna and lumbar puncture intrathecal delivery of AAV9 in mice to treat neuropathies. *Brain Res.* **2020**, *1739*, 146832. [CrossRef]
30. Chandran, J.; Chowdhury, E.A.; Perkinton, M.; Jamier, T.; Sutton, D.; Wu, S.; Dobson, C.; Shah, D.K.; Chessell, I.; Meno-Tetang, G.M.L. Assessment of AAV9 distribution and transduction in rats after administration through Intrastriatal, Intracisterna magna and Lumbar Intrathecal routes. *Gene Ther.* **2023**, *30*, 132–141. [CrossRef]
31. Armbruster, N.; Lattanzi, A.; Jeavons, M.; Van Wittenberghe, L.; Gjata, B.; Marais, T.; Martin, S.; Vignaud, A.; Voit, T.; Mavilio, F.; et al. Efficacy and biodistribution analysis of intracerebroventricular administration of an optimized scAAV9-SMN1 vector in a mouse model of spinal muscular atrophy. *Mol. Ther. Methods Clin. Dev.* **2016**, *3*, 16060. [CrossRef] [PubMed]
32. Ohno, K.; Samaranch, L.; Hadaczek, P.; Bringas, J.R.; Allen, P.C.; Sudhakar, V.; Stockinger, D.E.; Snieckus, C.; Campagna, M.V.; San Sebastian, W.; et al. Kinetics and MR-Based Monitoring of AAV9 Vector Delivery into Cerebrospinal Fluid of Nonhuman Primates. *Mol. Ther. Methods Clin. Dev.* **2019**, *13*, 47–54. [CrossRef] [PubMed]
33. Corti, M.; Byrne, B.J.; Gessler, D.J.; Thompson, G.; Norman, S.; Lammers, J.; Coleman, K.E.; Liberati, C.; Elder, M.E.; Escolar, M.L.; et al. Adeno-associated virus-mediated gene therapy in a patient with Canavan disease using dual routes of administration and immune modulation. *Mol. Ther. Methods Clin. Dev.* **2023**, *30*, 303–314. [CrossRef]
34. Bostick, B.; Ghosh, A.; Yue, Y.; Long, C.; Duan, D. Systemic AAV-9 transduction in mice is influenced by animal age but not by the route of administration. *Gene Ther.* **2007**, *14*, 1605–1609. [CrossRef]
35. Byrne, L.C.; Lin, Y.J.; Lee, T.; Schaffer, D.V.; Flannery, J.G. The expression pattern of systemically injected AAV9 in the developing mouse retina is determined by age. *Mol. Ther.* **2015**, *23*, 290–296. [CrossRef]
36. Gray, S.J.; Foti, S.B.; Schwartz, J.W.; Bachaboina, L.; Taylor-Blake, B.; Coleman, J.; Ehlers, M.D.; Zylka, M.J.; McCown, T.J.; Samulski, R.J. Optimizing promoters for recombinant adeno-associated virus-mediated gene expression in the peripheral and central nervous system using self-complementary vectors. *Hum. Gene Ther.* **2011**, *22*, 1143–1153. [CrossRef]
37. Grieger, J.C.; Soltys, S.M.; Samulski, R.J. Production of Recombinant Adeno-associated Virus Vectors Using Suspension HEK293 Cells and Continuous Harvest of Vector from the Culture Media for GMP FIX and FLT1 Clinical Vector. *Mol. Ther.* **2016**, *24*, 287–297. [CrossRef]
38. Boitnott, A.; Rioux, M.; Chen, X.; Gray, S. Lumbar Intrathecal Injection of Gene Therapy Vectors for Central Nervous System Targeting in Mice and Rats. *J. Vis. Exp.* **2025**, *219*, e67138. [CrossRef]
39. Glascock, J.J.; Osman, E.Y.; Coady, T.H.; Rose, F.F.; Shababi, M.; Lorson, C.L. Delivery of therapeutic agents through intracerebroventricular (ICV) and intravenous (IV) injection in mice. *J. Vis. Exp.* **2011**, *56*, e2968. [CrossRef]
40. Pardridge, W.M. CSF, blood-brain barrier, and brain drug delivery. *Expert Opin. Drug Deliv.* **2016**, *13*, 963–975. [CrossRef]
41. Sheehan, D.C.; Hrapchak, B.B. *Theory and Practice of Histotechnology*, 2nd ed.; C.V. Mosby: St. Louis, MO, USA, 1980.
42. Woods, A.E.; Ellis, R.C. *Laboratory Histopathology: A Complete Reference*; Churchill Livingstone: Edinburgh, Scotland, 1994.
43. Hinderer, C.; Katz, N.; Buza, E.L.; Dyer, C.; Goode, T.; Bell, P.; Richman, L.K.; Wilson, J.M. Severe Toxicity in Nonhuman Primates and Piglets Following High-Dose Intravenous Administration of an Adeno-Associated Virus Vector Expressing Human SMN. *Hum. Gene Ther.* **2018**, *29*, 285–298. [CrossRef]
44. Hordeaux, J.; Buza, E.L.; Dyer, C.; Goode, T.; Mitchell, T.W.; Richman, L.; Denton, N.; Hinderer, C.; Katz, N.; Schmid, R.; et al. Adeno-Associated Virus-Induced Dorsal Root Ganglion Pathology. *Hum. Gene Ther.* **2020**, *31*, 808–818. [CrossRef]
45. Hordeaux, J.; Buza, E.L.; Jeffrey, B.; Song, C.; Jahan, T.; Yuan, Y.; Zhu, Y.; Bell, P.; Li, M.; Chichester, J.A.; et al. MicroRNA-mediated inhibition of transgene expression reduces dorsal root ganglion toxicity by AAV vectors in primates. *Sci. Transl. Med.* **2020**, *12*, eaba9188. [CrossRef]
46. Chen, X.; Dong, T.; Hu, Y.; De Pace, R.; Mattera, R.; Eberhardt, K.; Ziegler, M.; Pirovolakis, T.; Sahin, M.; Bonifacino, J.S.; et al. Intrathecal AAV9/AP4M1 gene therapy for hereditary spastic paraplegia 50 shows safety and efficacy in preclinical studies. *J. Clin. Investig.* **2023**, *133*, e164575. [CrossRef] [PubMed]
47. Beard, H.; Winner, L.; Shoubridge, A.; Parkinson-Lawrence, E.; Lau, A.A.; Mubarokah, S.N.; Lance, T.R.; King, B.; Scott, W.; Snel, M.F.; et al. Evaluation of neuroretina following i.v. or intra-CSF AAV9 gene replacement in mice with MPS IIIA, a childhood dementia. *CNS Neurosci. Ther.* **2024**, *30*, e14919. [CrossRef] [PubMed]
48. Belov, V.; Appleton, J.; Levin, S.; Giffenig, P.; Durcanova, B.; Papisov, M. Large-Volume Intrathecal Administrations: Impact on CSF Pressure and Safety Implications. *Front. Neurosci.* **2021**, *15*, 604197. [CrossRef] [PubMed]
49. Moazen, M.; Alazmani, A.; Rafferty, K.; Liu, Z.J.; Gustafson, J.; Cunningham, M.L.; Fagan, M.J.; Herring, S.W. Intracranial pressure changes during mouse development. *J. Biomech.* **2016**, *49*, 123–126. [CrossRef]
50. Marco, S.; Haurigot, V.; Jaen, M.L.; Ribera, A.; Sanchez, V.; Molas, M.; Garcia, M.; Leon, X.; Roca, C.; Sanchez, X.; et al. Seven-year follow-up of durability and safety of AAV CNS gene therapy for a lysosomal storage disorder in a large animal. *Mol. Ther. Methods Clin. Dev.* **2021**, *23*, 370–389. [CrossRef]
51. Ansari, A.M.; Ahmed, A.K.; Matsangos, A.E.; Lay, F.; Born, L.J.; Marti, G.; Harmon, J.W.; Sun, Z. Cellular GFP Toxicity and Immunogenicity: Potential Confounders in in Vivo Cell Tracking Experiments. *Stem Cell Rev. Rep.* **2016**, *12*, 553–559. [CrossRef]

52. Khabou, H.; Cordeau, C.; Pacot, L.; Fisson, S.; Dalkara, D. Dosage Thresholds and Influence of Transgene Cassette in Adeno-Associated Virus-Related Toxicity. *Hum. Gene Ther.* **2018**, *29*, 1235–1241. [CrossRef]
53. Chen, X.; Dong, T.; Hu, Y.; Shaffo, F.C.; Belur, N.R.; Mazzulli, J.R.; Gray, S.J. AAV9/MFSD8 gene therapy is effective in preclinical models of neuronal ceroid lipofuscinosis type 7 disease. *J. Clin. Investig.* **2022**, *132*, e146286. [CrossRef]
54. Presa, M.; Bailey, R.M.; Davis, C.; Murphy, T.; Cook, J.; Walls, R.; Wilpan, H.; Bogdanik, L.; Lenk, G.M.; Burgess, R.W.; et al. AAV9-mediated FIG4 delivery prolongs life span in Charcot-Marie-Tooth disease type 4J mouse model. *J. Clin. Investig.* **2021**, *131*, e137159. [CrossRef]
55. Boitnott, A.; Jiji, A.; Plautz, E.J.; Hu, Y.; Chen, X.; Gray, S.J. Exploration of a DDX3X Gene Supplementation Therapy Including Expanded Characterization and Novel Findings of Sleep Disturbances in Ddx3x Haploinsufficient Mice. *Biol. Psychiatry Glob. Open Sci.* **2025**, *5*, 100599. [CrossRef] [PubMed]
56. Sinnett, S.E.; Hector, R.D.; Gadalla, K.K.E.; Heindel, C.; Chen, D.; Zaric, V.; Bailey, M.E.S.; Cobb, S.R.; Gray, S.J. Improved MECP2 Gene Therapy Extends the Survival of MeCP2-Null Mice without Apparent Toxicity after Intracisternal Delivery. *Mol. Ther. Methods Clin. Dev.* **2017**, *5*, 106–115. [CrossRef]
57. Van Alstyne, M.; Tattoli, I.; Delestree, N.; Recinos, Y.; Workman, E.; Shihabuddin, L.S.; Zhang, C.; Mentis, G.Z.; Pellizzoni, L. Gain of toxic function by long-term AAV9-mediated SMN overexpression in the sensorimotor circuit. *Nat. Neurosci.* **2021**, *24*, 930–940. [CrossRef] [PubMed]
58. Xie, Q.; Chen, X.; Ma, H.; Zhu, Y.; Ma, Y.; Jalinous, L.; Cox, G.F.; Weaver, F.; Yang, J.; Kennedy, Z.; et al. Improved gene therapy for spinal muscular atrophy in mice using codon-optimized hSMN1 transgene and hSMN1 gene-derived promotor. *EMBO Mol. Med.* **2024**, *16*, 945–965. [CrossRef] [PubMed]
59. Gray, S.J.; Blake, B.L.; Criswell, H.E.; Nicolson, S.C.; Samulski, R.J.; McCown, T.J.; Li, W. Directed evolution of a novel adeno-associated virus (AAV) vector that crosses the seizure-compromised blood-brain barrier (BBB). *Mol. Ther.* **2010**, *18*, 570–578. [CrossRef]
60. Ling, Q.; Rioux, M.; Higgs, H.; Hu, Y.; Dwyer, S.E.; Gray, S.J. Improved AAV9-based gene therapy design for SURF1-related Leigh syndrome with minimal toxicity. *Mol. Ther. Methods Clin. Dev.* **2025**, *33*, 101554. [CrossRef] [PubMed]
61. Thouvenin, O.; Keiser, L.; Cantaut-Belarif, Y.; Carbo-Tano, M.; Verweij, F.; Jurisch-Yaksi, N.; Bardet, P.L.; van Niel, G.; Gallaire, F.; Wyart, C. Origin and role of the cerebrospinal fluid bidirectional flow in the central canal. *elife* **2020**, *9*, e47699. [CrossRef] [PubMed]
62. Semple, B.D.; Blomgren, K.; Gimlin, K.; Ferriero, D.M.; Noble-Haeusslein, L.J. Brain development in rodents and humans: Identifying benchmarks of maturation and vulnerability to injury across species. *Prog. Neurobiol.* **2013**, *106–107*, 1–16. [CrossRef] [PubMed]

Disclaimer/Publisher's Note: The statements, opinions and data contained in all publications are solely those of the individual author(s) and contributor(s) and not of MDPI and/or the editor(s). MDPI and/or the editor(s) disclaim responsibility for any injury to people or property resulting from any ideas, methods, instructions or products referred to in the content.